Lightweight and Efficient Manifold Design for Hydrogen Fuel Cell Powered Unmanned Aerial Vehicles (UAVs)

A Major Qualifying Project submitted to the Faculty of WORCESTER POLYTECHNIC INSTITUTE in partial fulfillment of the requirements for the Bachelor of Science

By:

Michael Bonito

Jack Cassidy

Liam Hemmerling

Sophia Islam

Avery Purtell

Submitted to:

Ahmet Can Sabuncu, Ph.D.

Sponsored By:

Honeywell Aerospace

Date:

April 25th, 2024

Abstract

This paper explores various strategies used to optimize the design of a manifold for housing a hydrogen proton exchange membrane fuel cell system for Honeywell Aerospace's Unmanned Aerial Vehicles (UAVs). By leveraging a manifold design, our team aimed to enhance power efficiency, while minimizing weight and volume. Nodes and pathways between nodes were analyzed by comparing weight and length, which guided informed design decisions for the manifold. Eventually, the manifolds were 3D printed using multi-jet printing with nylon to be tested on a Honeywell 600W UAV. Compared to the original system, our final design significantly reduced the weight, maximum extent volume, part count, and assembly time. With the rise in demand for sustainable energy solutions, hydrogen fuel cells offer promising prospects for mitigating climate change. Through meticulous investigation of component placement and pathway functionality, this project contributes to easier assembly of the fuel cell system, thus advancing clean energy applications.

List of Figures

List of Tables

Authorship Table

Section	Author (s)	Editor (s)
Introduction	Sophia Islam	AP
Proton Exchange Membrane Fuel Cell	Liam Hemmerling	AP
Anode Loop	Sophia Islam	LH
Cathode Loop	Michael Bonito	AP
Coolant Loop	Liam Hemmerling	AP
Electrical System	Liam Hemmerling	AP
Multi-Jet Fusion	Sophia Islam	AP
Goal Statement and Project Objectives	Jack Cassidy	SI
Design Objectives and Requirements	Sophia Islam	AP
Understanding Fuel Cell System	Michael Bonito	SI
Nodal Language and Block Diagrams	Michael Bonito	SI
Additive Manufacturing	Sophia Islam	AP
Design Process	Jack Cassidy	MB
Design Vision	Jack Cassidy	MB
Original Design Layout	Sophia Islam	MB
Optimized Design Layout	Avery Purtell	MB
Initial Design Concept	Avery Purtell	MB
Coolant and Cathode Manifold	Jack Cassidy	MB
Original Design	Jack Cassidy	MB
Coolant Manifold Iteration 1	Jack Cassidy	MB
Coolant Manifold Iteration 2	Jack Cassidy	MB
Coolant Manifold Iteration 3	Jack Cassidy	MB
Blower and Ballast Manifold	Liam Hemmerling	MB
Original Design	Liam Hemmerling	MB
Our Design Vision and Reason	Liam Hemmerling	MB
Blower Manifold Iteration 1	Liam Hemmerling	MB
Blower Manifold Iteration 2	Liam Hemmerling	MB
Blower Manifold Iteration 3	Liam Hemmerling	MB
PCB Mounting Frame	Sophia Islam	MB

Support Stand	Michael Bonito	SI
Final Iteration of Entire System	Jack Cassidy	MB
Results and Analysis	Jack Cassidy	SI
Geometric Fit Tests	Sophia Islam	MB
Hydrostatic Pressure Testing and Adjustments	Jack Cassidy, LH	SI
Final Testing and Results	Liam Hemmerling	SI
Final Design Comparison	Michael Bonito	SI, LH
Volume Reduction	Jack Cassidy	MB
Weight Reduction	Michael Bonito	SI
Pathway Reduction	Michael Bonito	SI
Part Reduction and Assembly	Michael Bonito	SI
Limitations	Sophia Islam	MB
Challenges with Maintenance	Avery Purtell	SI
Adaptability to Other Applications	Sophia Islam	MB
Difficulty of Assembly	Avery Purtell	SI
Accessibility to Residual Nylon Powder	Avery Purtell	SI
Design and Manufacturing Recommendations	Sophia Islam	MB
Conclusion	Michael Bonito	AP
Project Impact	Michael Bonito	SI
Economic Impact	Michael Bonito	SI
Environmental Impact	Michael Bonito	SI
Societal Impact	Michael Bonito	SI
Future Work	Michael Bonito, SI	SI

Contributions List

Contribution	Main Contributor (s)	Supporting
Nodal Pathway Process Flow Diagram	Michael Bonito, Sophia Islam	LH, JC, AP
Nodal Language Creation and Assignment	Michael Bonito, Liam Hemmerling, Sophia Islam, Avery Purtell	JC, AP, SI
Nodal Analysis	Michael Bonito, Liam Hemmerling, Sophia Islam, Avery Purtell	JC
CAD of original design layout	Jack Cassidy	LH, MB, AP, SI
Design and CAD of Coolant Manifold	Jack Cassidy	LH
Design and CAD of Blower and Ballast Manifold	Liam Hemmerling	SI
Design and CAD of PCB Mounting Board	Sophia Islam, Avery Purtell	JC
System Support Stand	Michael Bonito	LH
CAD Assembly of Final Components	Jack Cassidy	LH
Geometric Fit tests	Liam Hemmerling, Jack Cassidy	MB, SI, AP
Hydrostatic Pressure Testing	Michael Bonito, Jack Cassidy Liam Hemmerling, Avery Purtell	SI
Final Design Comparison	Michael Bonito, Liam Hemmerling	JC, SI, AP
BOM for optimized system	Michael Bonito	LH

1. Introduction

This paper will investigate an approach to optimize the design of a manifold for housing a hydrogen proton exchange membrane fuel cell system on an Unmanned Aerial Vehicles (UAV). A manifold is a general term for an element which can split or combine different flows, often used in engineering applications with fluid mechanics. A manifold design within the UAV system would allow for the maximization of power efficiency while reducing weight and volume within the system. Manifold designs are also helpful in minimizing pressure drops and obtaining more uniform flow. ("Optimization of Manifold Design for 1 kW-Class Flat-Tubular Solid Oxide Fuel Cell Stack Operating on Reformed Natural Gas," 2016).

The goals for this project are to improve flight time duration, increase energy density and reduce manufacturing labor. From systems analyses of the block diagrams, to critical evaluations of individual nodes, a top-down approach to automated design will offer the best solutions for optimizing the weight, volume, and power of the UAV. Optimization tools will be investigated, and Excel will be used to analyze nodes and identify critical areas of improvement. These tools will allow us to make educated decisions on the optimal design layouts to be 3D-printed and tested on Honeywell's 600W UAV.

Hydrogen fuel cells have gained popularity on the topic of sustainable energy as the demand for ways to mitigate climate change and reduce carbon emissions increases. The only byproducts of proton exchange membrane fuel cells (PEMFCs) are heat and water, making them ideal for clean energy production in vehicles, and a potential solution for combatting the environmental crisis faced today (Wang et al., 2024). The main advantage of this type of fuel cell is that they operate at low temperature and high current densities (Guerrero Moreno et al., 2015). The use of PEMFCs is commonly discussed in its application in electric vehicles, known as fuel cell electric vehicles (FCEVs). Other variations include fuel cell hybrid electric vehicles (FCHEVs) which offer even more advantages by offsetting the limitations of FCEVs. FCEVs offer high mileage, fast charging, quiet performance, and zero carbon emissions during use (Wang et al., 2024). The main cost within fuel cells comes from the bipolar plates, which connect the surface of one cathode and one anode to the next cell, and the Membrane Electrode Assembly (MEA), which is the central layer of polymer electrolyte membrane (PEM) between the two catalyst layers (CLs). Production costs for these fuel cell systems are generally high, but

there is room for reducing cost in these areas and within the proton-conducting membranes (Guerrero Moreno et al., 2015).

Research into clean energy has provided many options for minimizing the release of fossil fuels, but these options still require energy use through transportation and production. Hydrogen fuel cells appear to be a feasible and realistic solution to cleaner and more efficient energy, especially in UAVs. UAVs have seen major advancements in recent years as use spans across industries, from delivery services to military surveillance applications.

To approach this complex issue of optimizing a fuel cell system for a UAV, we first researched PEM fuel cells, the four loops of the UAV system, and biomimicry and its implementation in engineering. Using this information, we investigated the different pathways of fluid, gas, and their corresponding weights throughout the different loops of the UAV system. We then created a nodal language to analyze these pathways and ranked each pathway based on the optimization of weight and length. Block diagram layouts were created using the nodal analysis to identify different options for structuring the manifold and the locations of each component within the manifold. This selected layout was identified as the design which optimizes the total weight and pathway lengths. After choosing the best layout for the manifold, a 3D CAD model was created in SolidWorks, and the final CAD design was 3D printed using nylon multi-jet fusion technology. The 3D printed manifolds were then tested for fit and functionality by assembling the PEMFC system and running it. The goal of the optimized design is to increase the power efficiency while reducing hardware and installation time.

2. Background

Honeywell's 600-Watt UAV power system has many complex loops and systems that in combination, create a working fuel cell. Understanding the complex relationships between these systems is an integral part of being able to optimize the entire power system. It is also essential to understand the requirements and constraints of designing a manifold. The shape, volume, weight, and materials will all play key roles in the successful optimization of the layout and functionality of the UAV's power system, and the implementation of 3D printed manifold pieces. Hence, proper research went into understanding the processes in the PEMFC, the limitations of manifold design, and the fabrication techniques of additive manufacturing (AM).

2.1 Proton Exchange Membrane Fuel Cell

The UAV is powered by electricity generated from a proton exchange membrane fuel cell (PEMFC), which uses hydrogen gas as fuel. As displayed in the schematic of the PEMFC in Figure 1 below, the proton exchange membrane is typically made from a polymer membrane and requires sufficient ionic conductivity and low electrical conductivity. Air is provided to the cathode side of the PEMFC, as oxygen is required for the chemical reaction, exhibited in the equation below. Hydrogen gas is provided to the anode side, the hydrogen atoms are ionized, and the ions are conducted through the proton exchange membrane. The electrons stripped from the nucleus are free to be used for the motors providing thrust to the UAV. The oxygen and hydrogen ions combine at the cathode to produce H_2O molecules (water) as a waste product, shown in the chemical reaction in Equation 1 (Kraytsberg & Ein-Eli, 2014).

$$2\,H_2 + O_2 \xrightarrow{yields} 2\,H_2O + 2e^- \qquad [1]$$

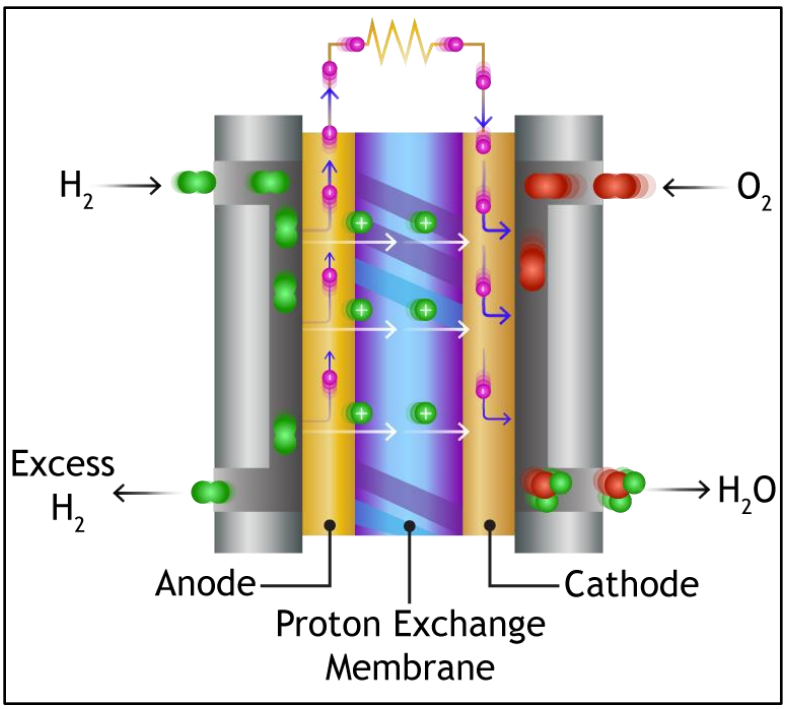

Figure 1: A Proton Exchange Membrane schematic (PEM Fuel Cells).

The PEMFC has four systems, or loops, that allow the fuel cell stack to function properly. These four loops, shown in Figure 2, are the anode loop, cathode loop, coolant loop and the electrical system.

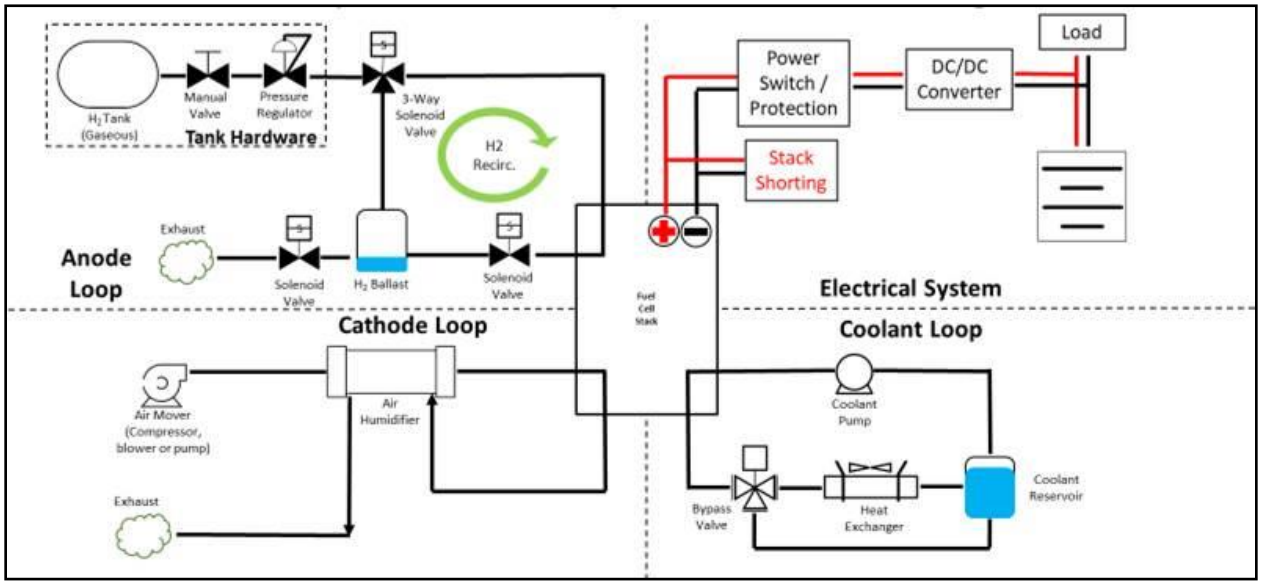

Figure 2: Block diagram schematic of the entire UAV system including the four loops.

The anode loop is where the hydrogen enters the PEMFC and contains the purge assembly system to regulate the fuel cell. The cathode loop provides air to the fuel cell and regulates the moisture content within the fuel cell. The coolant loop is used to cool the system and properly regulate the system to an ideal temperature of 62°C. Lastly, the electrical system contains the PCB which controls the other loops while also managing the power output from the stack assembly.

2.1.1 Anode Loop

The anode loop is responsible for providing hydrogen gas (H_2) to the fuel cell stack, at which point it is ionized as it moves across the anode. This ionization process provides the electrons for the electrical load and battery to charge within the electrical system (described in detail in Section 2.1.3). The anode loop is composed of a hydrogen tank, a pressure regulator, solenoid valves, and a hydrogen ballast, as shown in Figure 3.

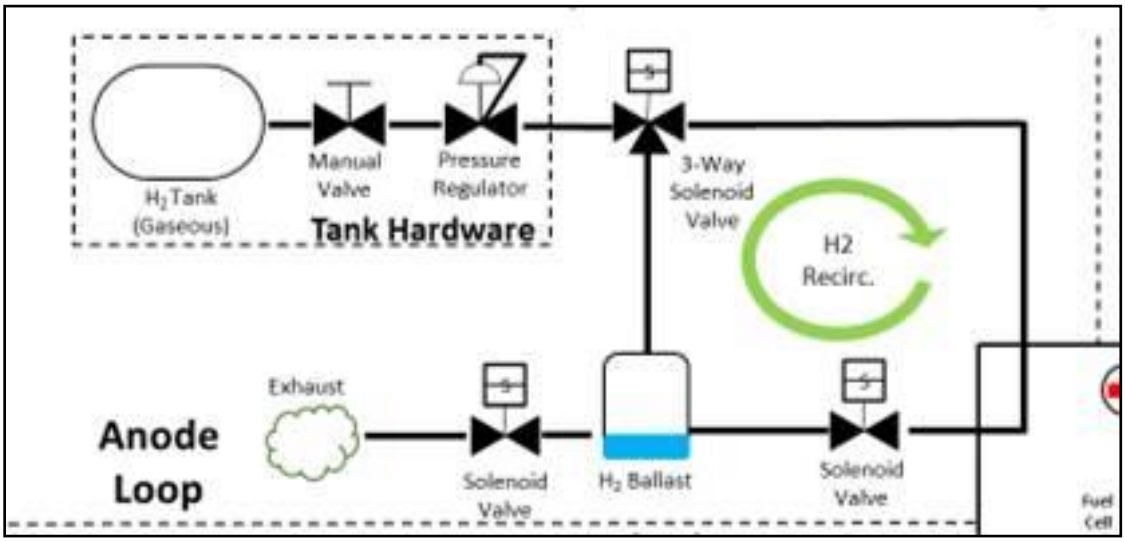

Figure 3: Close-up schematic of the anode loop, including the tank, solenoid valves, and ballast.

The flow of hydrogen starts in the pressurized hydrogen tank and flows through the pressure regulator where the pressure is reduced from 6000 psi to about 15 psi. The hydrogen then enters the fuel cell stack after it passes through a 3-way solenoid valve. The control system determines when the hydrogen within the fuel cell has been adequately used, at which point it passes into the ballast. The purpose of the ballast is to ensure there is no water build-up within the stack and to ensure that the hydrogen is mostly, or all used before it is exhausted. This ensures that there are no contaminants in the hydrogen gas stream that can build up in the fuel

cell causing a power gradience. Once the hydrogen enters the ballast, it can either be exhausted with any water or impurities in the ballast, or recirculated back through the stack once the water has been removed to the ballast. This process allows more of the hydrogen gas to be used, while maintaining proper water content in the stack.

2.1.2 Cathode Loop

The cathode loop is responsible for providing oxygen to the fuel cell stack and maintaining a proper moisture content within the fuel cell stack. The cathode loop is primarily composed of an air pump and an air humidifier as shown in Figure 4. Air containing oxygen, nitrogen, and other gases and particles, flows through an air filter before being moved by the blower into the humidifier.

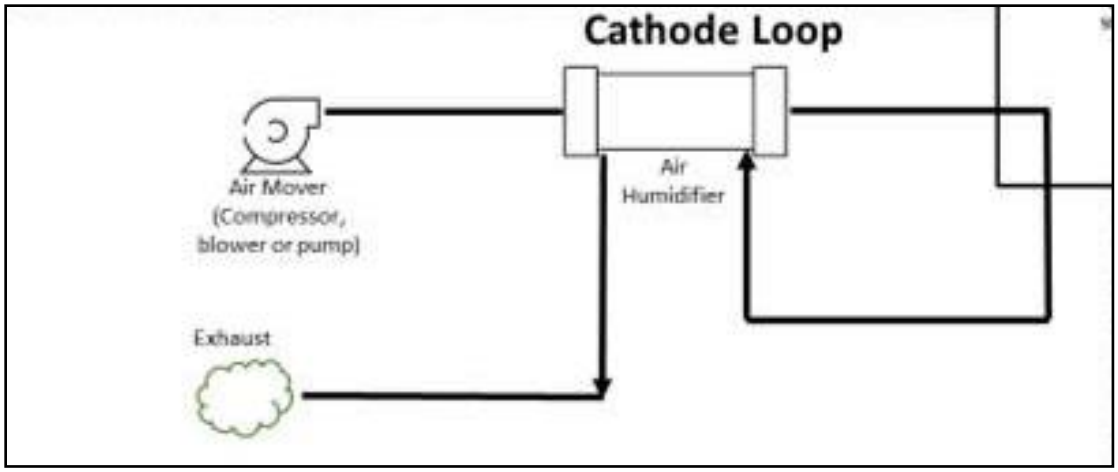

Figure 4: Close-up schematic of the cathode loop, including the air blower and humidifier.

In the humidifier, the inlet air is humidified, and excess water is removed from the loop through the exhaust outlet. Humidifying the air is important because it ensures the fuel cell stack does not dry out. The humidifying process is achieved by taking excess water byproduct from the chemical process described in Equation 1 and putting it through the humidifier. The humidifier in this PEMFC system contains a Nafion tubing water exchanger, which is an effective agent for humidifying air. Nafion is a polymer that allows water to permeate through to humidify the incoming air. This allows gas and fluid streams to mix upon entering the humidifier, while only permitting the humidified air to pass through to the stack. Nafion is also useful for maximizing surface areas and handling high pressures.

Because the air entering the system is not purely oxygen, the blower moves an excess amount of air into the system to ensure that there is enough oxygen to combine with the hydrogen for the chemical reaction that occurs within the fuel cell stack.

2.1.3 Coolant Loop

The coolant loop is responsible for cooling the system and preventing it from overheating. Excessive operating temperatures dry out the membrane and reduce the catalyst surface area, negatively impacting efficiency. For every Watt of electrical power, about a Watt of heat is produced that must be taken out of the system. To do this, the coolant loop utilizes liquid cooling that passes between each "cell" in the fuel cell stack. The subsystem is composed of a coolant pump, a coolant reservoir, a fin and tube heat exchanger, and a pressure bypass valve as shown in Figure 5.

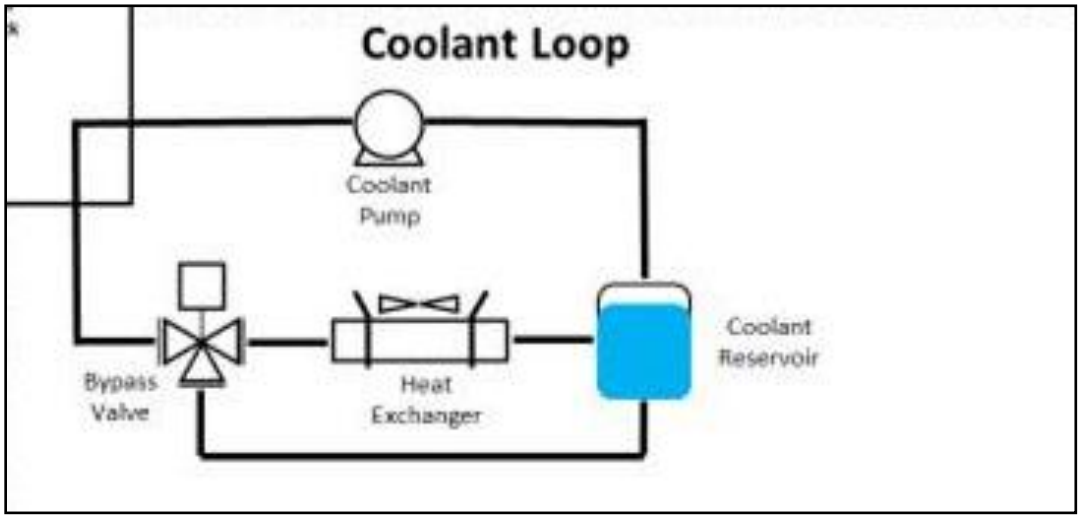

Figure 5: Close-up schematic of the coolant loop, including its components.

The coolant is pressurized by the coolant pump, which is fed from the reservoir. The pressurized coolant passes through the fuel cell stack and heat is conductively transferred to the liquid. The coolant exits the fuel cell stack and is directed through a temperature bypass valve and into the fin and tube heat exchanger. The bypass valve sends the hot coolant into the heat exchanger if the temperature is too high. If the temperature of the liquid entering the bypass valve is below the ideal operating temperature, the bypass valve will direct the coolant back to the reservoir and effectively "skipping" the heat exchanger. The heated coolant which flows through the tubes of the heat exchanger heats the fins by conduction which are then cooled by

convection with the ambient air. The coolant is then returned to the coolant reservoir after it has been cooled by the heat exchanger.

Pressure loss and water weight are important factors to consider when optimizing the coolant loop. Pressure loss can be found through any tube length, but especially within the fuel cell stack and heat exchanger where pressure loss is most noticeable. The cooling pathways within the PEMFC can be modeled as parallel flow paths which increase the conductive area between the coolant and the PEMFC. Similarly, the pathways within the heat exchanger are parallel flow paths, also used to increase the area of conduction between the coolant and the tubes of the heat exchanger. The mass flow rate of the coolant within both the PEMFC and heat exchanger relate to how much heat is added or removed from the coolant and can be related back to the supplied pressure from the coolant pump. A smaller mass flow rate of the coolant can be equated to more heat added/removed from the same amount of coolant, but at the cost of diminishing returns on efficiency as the mass flow rate is lowered.

The liquid cooling system allows the UAV to operate with ambient air temperatures between 5°C to 45°C, elevation between 0 feet and 15,000 feet above sea level, and relative humidity of the ambient air between 0 and 100% (*600U Hydrogen Fuel Cell,* 2021).

2.1.4 Electrical System

The electrical system is responsible for transmitting the electrical current created by the PEMFC to the load of the motors and charging the battery of the UAV. The electrical system consists of copper wire, a power switch, a DC-to-DC power converter, 6 motors powering the propeller blades, and a battery to consume additional power. A schematic of this electrical system is shown below in Figure 6.

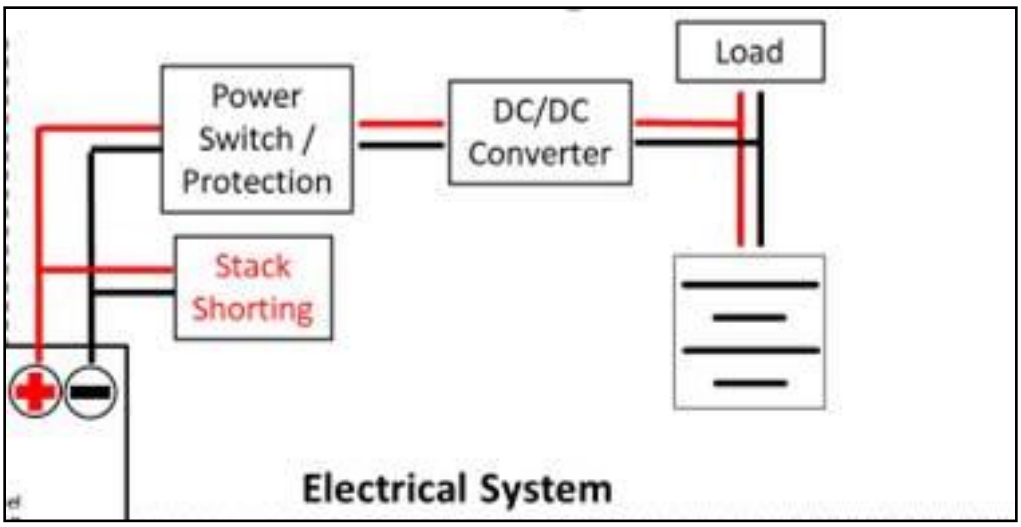

Figure 6: Close-Up schematic of the electrical system including its components.

The PEMFC produces about 30 amps continuously, with a peak power output of about 50 amps (*600U Hydrogen Fuel Cell*, 2021). The wires are attached to the PEMFC at the cathode and anode, from which they go through the power switch and into the DC/DC converter. The current is then supplied to each of the motors. Any power not used by the motors is used to charge the UAV's batteries.

The weight of the high current wires and appropriate battery size are important factors to consider when optimizing the electrical system.

2.2 Additive Manufacturing (AM) Techniques

2.2.1 Multi-Jet Fusion

When attempting to increase the power efficiency of the system, weight is an important factor to consider. Currently, the lift capacity of the drone is underwhelming and could be improved in future designs. There are several ways of reducing the weight of a UAV, especially when redesigning the structure of the system using additive manufacturing (AM).

One method is known as multi-jet fusion (MJF) additive manufacturing, which is a recent AM technology that allows for decrease of build-time without sacrificing strength and quality of the print. This method was developed by HP and involves powder bed fusion, in which polymer particles are heated and fused to fabricate parts. Specifically, our group will explore the options when using nylon, also called polyamide, in the MJF AM processes because this material is very

tough, abrasion resistant, and impact resistant, thus making it ideal for a wide range of applications. PA12, which is a general-use plastic used by injection molders, is the most widely used in MJF due to its high crystallization temperature and generally higher mechanical performance (O'Connor et al., 2018).

The multi-jet fusion additive manufacturing process is illustrated in Figure 7 below. First, a layer of PA powder is deposited onto the build platform and a fusing agent is applied to the powder bed. A detailing agent is applied to the powder bed to prevent fusion of particles. The polymer is then heated by passing infrared lamps over the bed and the fusing agent converts IR radiation into thermal energy. This fuses the polymer, which forms a layer. This is repeated as each layer is formed (O'Connor et al., 2018).

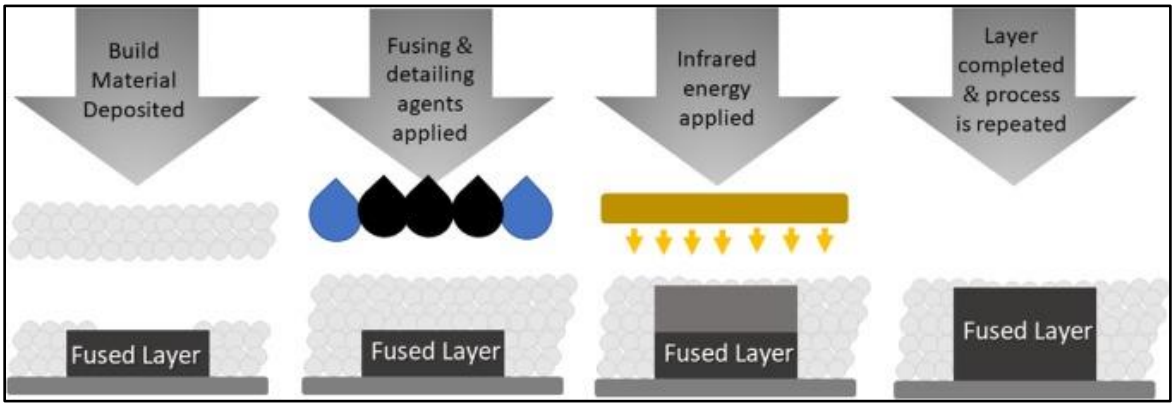

Figure 7: Schematic of the MJF process with polymer powder layer and fusing agent.

The process of MJF additive manufacturing allows for the kind of improved strength and quality of the product that our design will require. The manifold will contain complex pathways that transport various fluids, resulting in a need for smooth interior surfaces. There are two material options for nylon within the MJF process: PA 12 Black and PA 12 40% Glass-Filled Black. Our team will use PA12 black because of its near isotropic mechanical properties, as well as economic benefits. Another design requirement to consider is the tolerance of printed parts and the need for the manifold to pass a geometric fit test with the fuel cell system. MultiJet Fusion 3D printers have a maximum part size of 284x380x380mm and produce parts with tolerances of +/-0.3mm, which is ideal for this manufacturing need. The manifold also must high pressures, and the tensile strength of this material is 7.1ksi, which fits our design requirements. When MJF is used, final parts will have quality surface finishes, fine feature resolution, and more consistent mechanical properties. This method will be very beneficial to us, especially as

we explore the proper materials, including fusing and detailing agents, to apply as it is printed to optimize the design.

3. Methodology

3.1 Goal Statement and Project Objectives

This chapter will reflect the team's strategy for completing the project to satisfy the design goals of the sponsor, Honeywell. The goal of this project was to design a fluid and gas distribution apparatus for a fuel cell system in Unmanned Aerial Vehicles (UAVs) by exchanging components and altering pathway configurations to minimize power losses, weight and volume while maintaining reliability and long-range capabilities.

Project Objectives necessary to achieve this goal include:

1. Create a "language" for understanding the nodal connections of the fuel cell system.
2. Create block diagram layouts for best approaches to optimizing fuel cell system.
3. Rank pathways and nodes based on weight and length.
4. Produce design layout options for fuel cell system based on pathways rankings and nodal analysis.
5. Design iterations for manifold piece for fuel cell system around optimal layout option.
6. 3D prints initial design iterations using resin printers and modify designs based on geometric fit tests.
7. 3D-print prototypes of manifolds using nylon multi-jet fusion printing and conduct geometric fit tests and hydrostatic pressure tests within the system.
8. Modify manifold design based on testing and 3D print final design using nylon in MultiJet fusion printing.

3.2 Design Objectives and Requirements

With our main goal being to make the new fuel cell system as compact as possible and eliminate excess hardware, we began the design process by identifying any requirements for the manifold. We created a list of qualitative objectives, then paired each objective with a quantitative design requirement to accomplish our goal. The design objectives and requirements can be seen in Table 1 below.

Table 1: Design Objectives and Requirements

Objectives	**Requirements**

Reduce tubing weight	• Reduce total tubing weight by at least 20%
Reduce length between pathways	• Reduce total tubing length by at least 20%
Reduce overall weight of the system	• Total end weight reduced by 20%
Reduce number of parts	• Number of components (screws, washers, nuts) reduced by at least 40% • Eliminate housing for components so all components are connected by one or two pieces
Standardize hardware to reduce number of tools needed for assembly	• Minimize number of different screws by at least 30% • Minimize fasteners and replace with snap fits or adhesives where possible
Reduce maximum extent volume of the entire system	• Make entire system more compact by designing one or two manifold pieces to replace components • Reduce maximum extent volume by at least 30%
Reduce labor cost for assembly of system	• Amount of time to assembly system will be reduced by at least 20% • Consider assembly processes to reduce time and effort for assembly
Optimize design for manufacturability of the system	• Simplify part geometries and designs to reduce complexity • Eliminate redundant or unnecessary components and features • Design multifunctional manifold parts

3.3 Understanding Fuel Cell System

The PEM Fuel Cell system is composed of four subsystems: the anode loop, the cathode loop, the electrical system, and the coolant loop. To effectively optimize the system, we first had to thoroughly understand each component within each loop, the pathways between components, and the relationships between components and pathways.

3.3.1 Nodal Language and Block Diagrams

In preparation for determining the best options for optimizing the fuel cell, a nodal "language" was created using block diagrams to better understand the relationships between each

loop and the fluid transfer between them. This language is documented for each pathway and component in Table 1 below.

Table 2: Nodal language codes and corresponding definitions

Loop	Type	Pathway Name	Nodal Code
Cathode	Component	Air Filter Inlet to Air Filter Outlet	C3A-C3B
Cathode	Pathway	Air Filter Outlet to Blower Inlet	C3B-C2A
Cathode	Component	Blower Inlet to Blower Outlet	C2A-C2B
Cathode	Pathway	Blower Outlet to Humidifier Inlet A	C2B-C1A
Cathode	Component	Humidifier Inlet A to Humdifier Outlet B	C1A-C1B
Cathode	Pathway	Humidifier Outlet B to Stack Inlet A	C1B-S1A
Cathode	Component	Stack Inlet A to Stack Outlet B	S1A-S1B
Cathode	Pathway	Stack Outlet B to Humidifier Inlet C	S1B-C1C
Cathode	Component	Humidifier Inlet C to Humdifier Outlet D	C1C-C1D
Cathode	Pathway	Humidifier Outlet D to Exhaust	C1D-C4
Coolant	Pathway	Pump Outlet to Bypass Valve Inlet	L1C-L2C
Coolant	Component	Bypass Valve Inlet to Bypass Valve Outlet B	L2C-L2B
Coolant	Pathway	Bypass Valve Outlet B to Heat Exchanger Inlet	L2B-L3A
Coolant	Component	Heat Exchanger Inlet to Heat Exchanger Outlet	L3A-L3B
Coolant	Pathway	Heat Exchanger Outlet to Reservoir Inlet	L3B-L4A
Coolant	Component	Reservoir Inlet to Reservoir Outlet	L4A-L4B
Coolant	Pathway	Reservoir Outlet to Pump Inlet B	L4B-L1B
Coolant	Component	Pump Inlet B to Pump Outlet	L1B-L1C
Coolant	Component	Bypass Valve Inlet C to Bypass Valve Outlet A	L2C-L2A
Coolant	Pathway	Bypass Valve Outlet A to Stack Inlet E	L2A-S1E
Coolant	Component	Stack Inlet E to Stack Outlet F	S1E-S1F
Coolant	Pathway	Stack Outlet F to Pump Inlet A	S1F-L1A
Anode	Component	Tank Hardware Inlet to Tank Hardware Outlet	A1A-A1B
Anode	Pathway	Tank Hardware Outlet to 3-Way Solenoid Valve Inlet A	A1B-A2A
Anode	Component	3-Way Solenoid Valve Inlet A to 3-Way Solenoid Valve Outlet B	A2A-A2B
Anode	Pathway	3-Way Solenoid Valve Outlet B to Stack Inlet C	A2B-S1C
Anode	Component	Stack Inlet C to Stack Outlet D	S1C-S1D
Anode	Pathway	Stack Outlet D to Solenoid Valve Inlet A	S1D-A3A
Anode	Component	Solenoid Valve Inlet to Solenoid Valve Outlet	A3A-A3B
Anode	Pathway	Solenoid Valve Outlet to Hydrogen Ballast Inlet	A3B-A4A
Anode	Component	Hydrogen Ballast Inlet to Hydrogen Ballast Outlet B	A4A-A4B
Anode	Pathway	Hydrogen Ballast Outlet B to Solenoid Valve Inlet	A4B-A5A
Anode	Component	Solenoid Valve Inlet to Solenoid Valve Outlet	A5A-A5B
Anode	Pathway	Solenoid Valve Outlet to Exhaust	A5B-A6A
Anode	Pathway	Hydrogen Ballast Outlet C to 3-Way Solenoid Valve Inlet C	A4C-A2C
Electrical	Component	Printed Circuit Board (PCB)	E1A-E1B

Each node is represented by a “code” corresponding to a definition, as shown in the table. The first letter corresponds to the loop, the number corresponds to the subcomponent, and the second letter corresponds to the inlet or outlet of the subcomponent. For example, “Air Filter Outlet” is represented by the nodal code, “C3B.” The letter “C” corresponds to the cathode loop, the number “3” corresponds to the air filter, and the second letter, “B,” corresponds to the outlet of the air filter subcomponent (Figure 8). For a complete nodal key for each individual node and each pathway, see Appendix I and II.

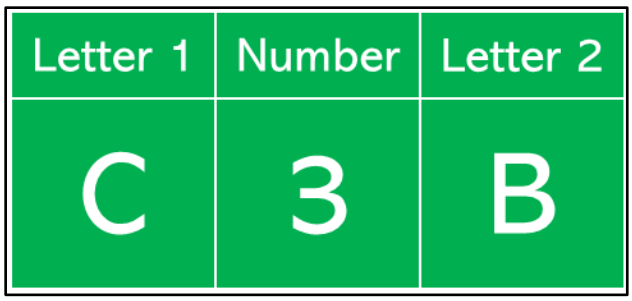

Figure 8: Nodal language code, "C3B," representing the "air filter outlet."

Each nodal code can be found on the diagram below to better understand the locations and pathways between components (Figure 9).

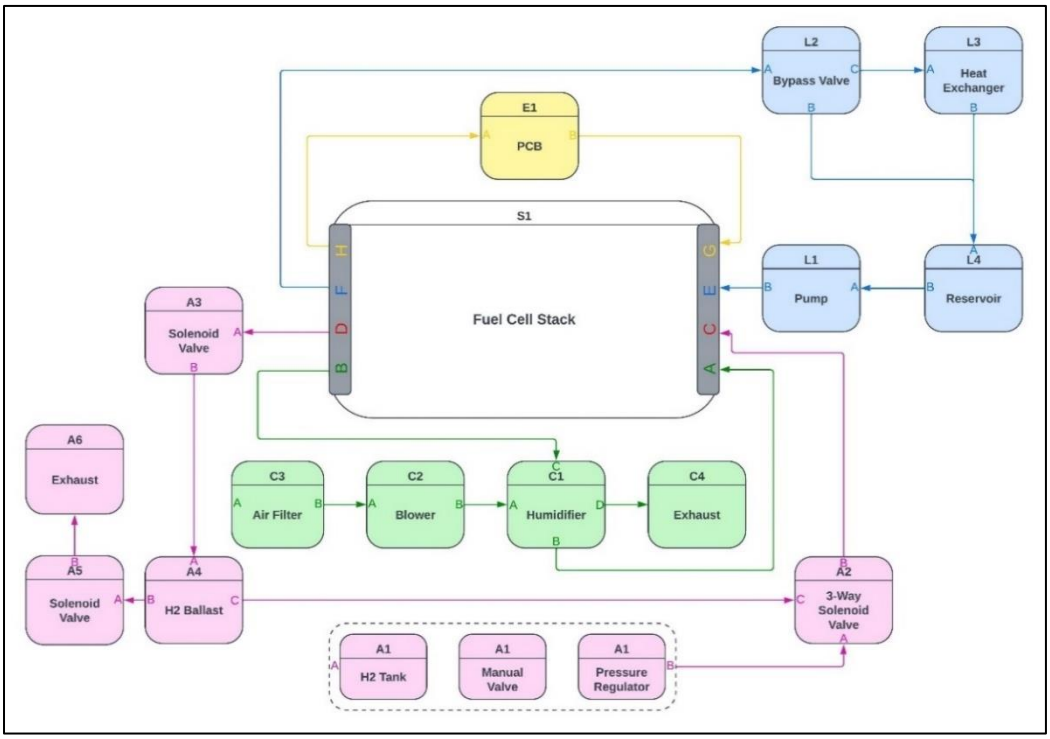

Figure 9: Block diagram representation of nodal language and pathways.

3.3.2 Nodal Analysis and Topographic Maps

After creating a coded language to identify and relate each component and pathway, the pathways were ranked according to subjective decisions based on the nodal analysis of the block diagram. Decisions reflected the overall goal of decreasing the weight and volume of the entire fuel cell system, which in turn, helps increase the power density of the system. This required investigating of the effects of variations in distances between certain nodes, sizes, and intricacies

of part configurations, along with the overall impact of weight and volume reduction that each node has on the system.

The lengths of pathways were taken from the assembly guide specification for each tube length. These measurements were then compiled in excel to be analyzed further. We created multiple bar graphs that compare the total lengths and weights of each of the pathways between the anode, cathode, and coolant loops. Figure 10 shows that the total lengths of pathways for the anode and coolant loops are almost double the total length of the pathways for the cathode loop. These lengths represent approximate calculations of the tubing between components. Some of the components were directly attached to one another and did not require tubing. Hence, they were not included in the chart because these pathways have no measurable length (Figure 10).

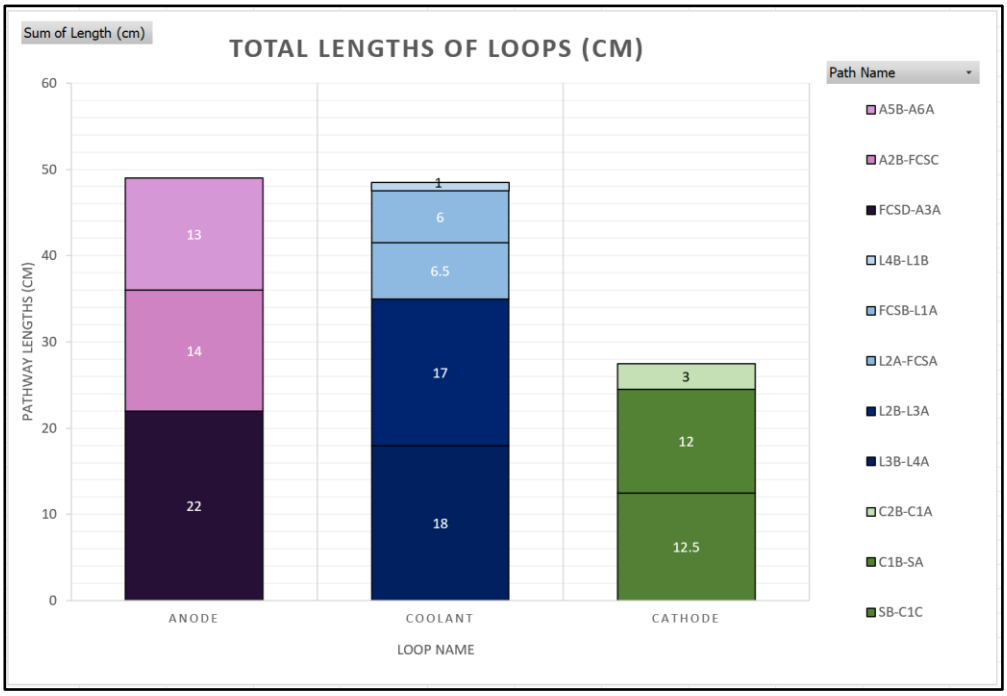

Figure 10: Bar graph of the total lengths of loops in centimeters.

The weight per length of tubing in each loop was also measured and calculated using a scale and calipers. It was necessary to calculate the weight per length of tubing because each loop utilizes a different sized tube. The length of the tubing was measured using calipers and the weight using a scale. This process was conducted twice, and the average was taken to represent the weight per 1 unit of length of each tubing. The calculations were completed in Excel and a bar graph representation is displayed in Figure 11. The weight of the pathways in the coolant

loop is more than double the weight of both the anode and cathode loops. This means that the coolant loop is the most critical subsystem to focus on in terms of reduction in weight.

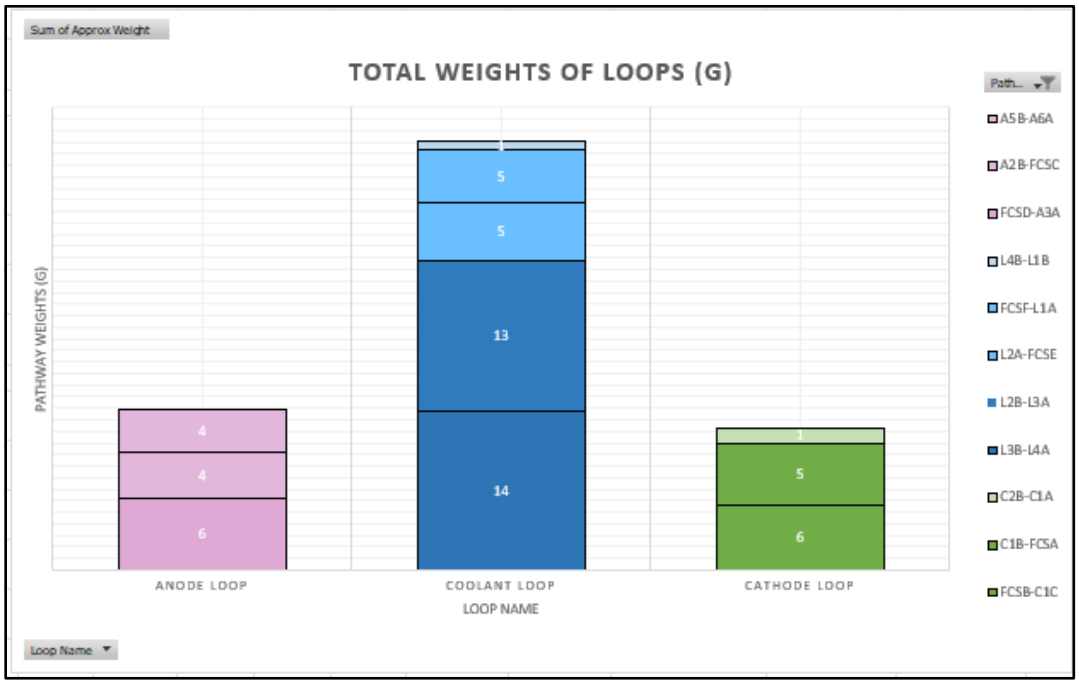

Figure 11: Bar graph of the total weights of loops in grams.

The analysis of nodal pathways informed our decisions by revealing which areas of the old design required the most prioritization for improvement. For example, we determined which pathways and loops contributed the greatest to the whole system's weight. Using this information, the team could make more informed design decisions to produce an optimal system design configuration. Once we have developed a complete understanding of the fuel cell system including its pathways and components, we will create an optimized manifold design using SolidWorks.

3.3 Additive Manufacturing Techniques

By modeling this kind of optimized manifold design in CAD software, we will be able to 3D print this part using additive manufacturing technologies. To create an optimized design, we will explore the option of a manifold design using additive manufacturing.

Original designs will be prototyped using WPI's 3D printers. These are Creality CR6-SE FDM 3D printers, which use Fused Deposition Modeling (FDM) and can print up to 235x235x250mm at 80-100mm/s. The team will use these printers for the preliminary prototypes

because they are cheaper and will allow us to generally see how the manifold design will function before finalizing it. These prototypes will also be crucial for testing purposes and analyzing how the design can be improved.

Once a final design is agreed upon, it will be printed using multi-jet fusion printers with nylon material. In our research on 3D printing technologies, we were guided towards Sicam's expertise in Multi Jet Fusion (MJF) printing. Using state-of-the-art HP 3D printers, Sicam delivers high-quality prototypes and production parts quickly and cost-effectively. Their MJF technology is ideal for small lot production without the need for costly tooling, making it a versatile solution for modern manufacturing needs. Additionally, Sicam's team provides valuable guidance to clients in choosing between MJF and SLA 3D printing, ensuring the most effective technology for each project. Overall, Sicam's innovative approach to MJF made it the perfect company to develop our parts.

4. Design Process

To tackle the design objectives within the constraints and produce a working fuel cell system prototype, our team created steps for our design process plan. In this section, we will introduce our coded nodal language used to relate and analyze pathways, discuss the creation of manifold configurations based on this analysis, and examine prototyping these designs.

The following is our design process:

1. Create 2D block diagrams to fully understand the fuel cell stack components.
2. Assemble components in CAD space.
3. Create initial manifold design concepts.
4. Iterate upon manifold design concepts based on design objectives and requirements.
5. 3D print initial manifold designs and test.

4.1 Design Vision

Having analyzed the shortcomings of the previous design, we embarked on conceptualizing a revamped manifold. Our design objectives centered around minimizing part count and decreasing overall volume and weight. To achieve these goals, we envisioned a manifold devoid of external tubing, consolidating multiple components into a singular unit. This integration not only streamlined the design but also minimized its overall footprint. Additionally, to optimize fluid flow and in turn, diminish pressure losses, we aimed to curtail the number of bends and turns in the fluid pathways.

By simplifying the part count, we aimed to enhance the user-friendliness of the fuel cell setup, making it less intricate and easier to assemble. Eliminating the need for plastic tubing would simplify assembly, requiring fewer tools and less expertise. Reducing the system's volume would enable the fuel cell to be accommodated in more confined spaces, while lowering the system's overall weight. Lastly, mitigating pressure loss would bolster system efficiency, enhancing the fuel cell's power generation capabilities and diminishing parasitic power losses.

4.2 Design Layout

4.2.1 Original Design Layout

The current design of Honeywell's 600W fuel cell system is not optimized with respect to weight, volume, and power efficiency. One area of improvement in the original design is the placement of components around the fuel cell stack, resulting in a large volume. Another factor is the long tubing pathways that cause large pressure losses. Finally, the excessive use of hardware such as fasteners and mounting plates added unnecessary weight. A top plane and bottom plane view are shown in Figure 12 and Figure 13, respectively.

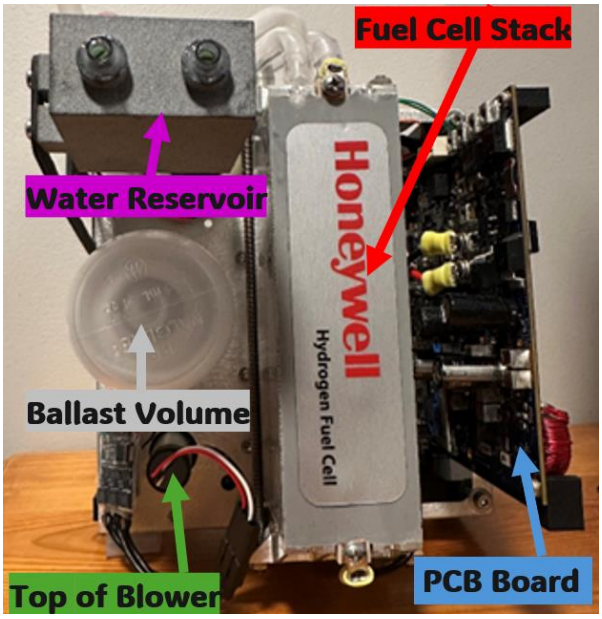

Figure 12: Image of top plane view of current design of fuel cell system.

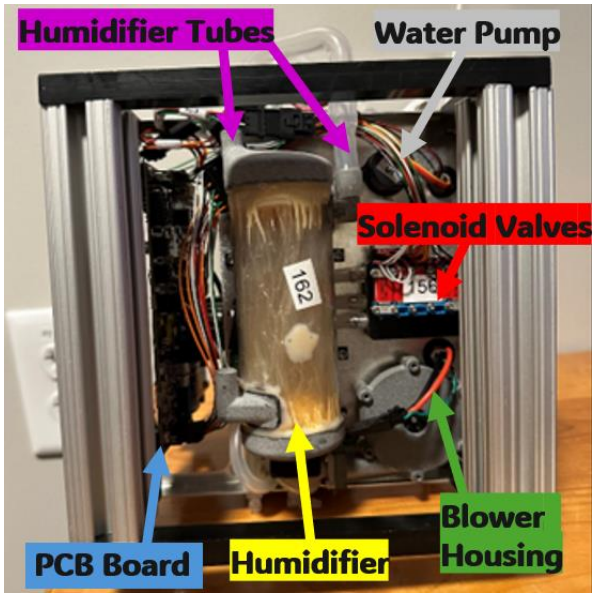

Figure 13: Image of bottom plane view of current design of fuel cell system.

A 2D model of the current design of the fuel cell system was created to represent the current layout and better understand the geometric configuration of the components (Figure 14).

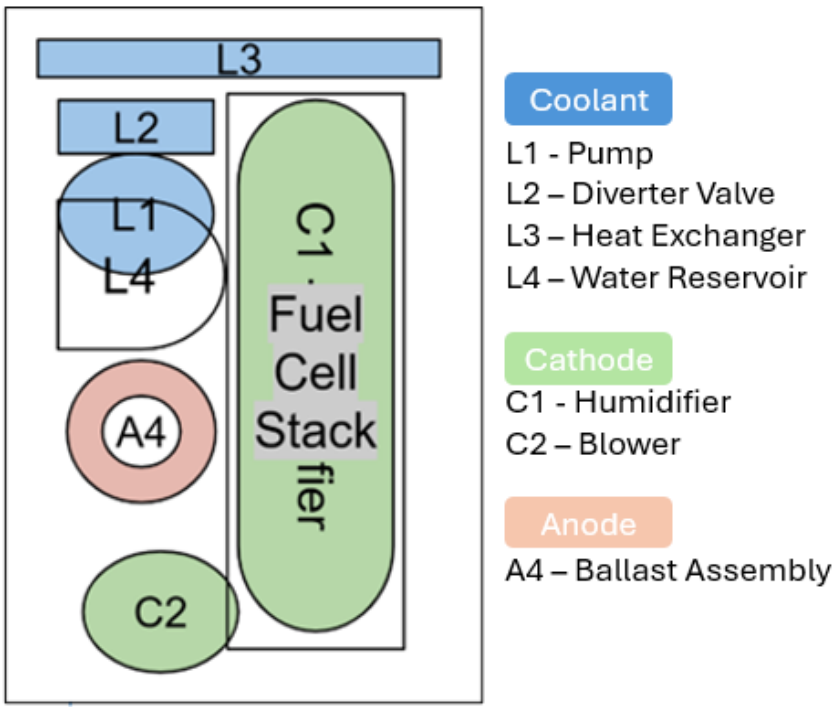

Figure 14: 2D model of current design layout of fuel cell system.

4.2.2 Optimized Design Layout

New design layouts were created with many factors contributing to the optimization of the fuel cell system. The proximity of certain components was considered to reduce pathway lengths and tubing weight. Geometric configurations were also considered to reduce the system's maximum extent volume and total volume.

Before modeling the potential design layout in CAD space, the team brainstormed optimal design configurations using 2D block diagrams. We settled on a configuration that reduced the most pathways, thus reducing tubing lengths, weight, and total volume (Figure 15). We focused our optimization specifically on the coolant loop, because this is where we identified the largest weight and tube lengths in the original design (discussed further in section 3.3.2). This 2D method was an easy way to visualize how to configure components without rushing into modeling in 3D CAD space.

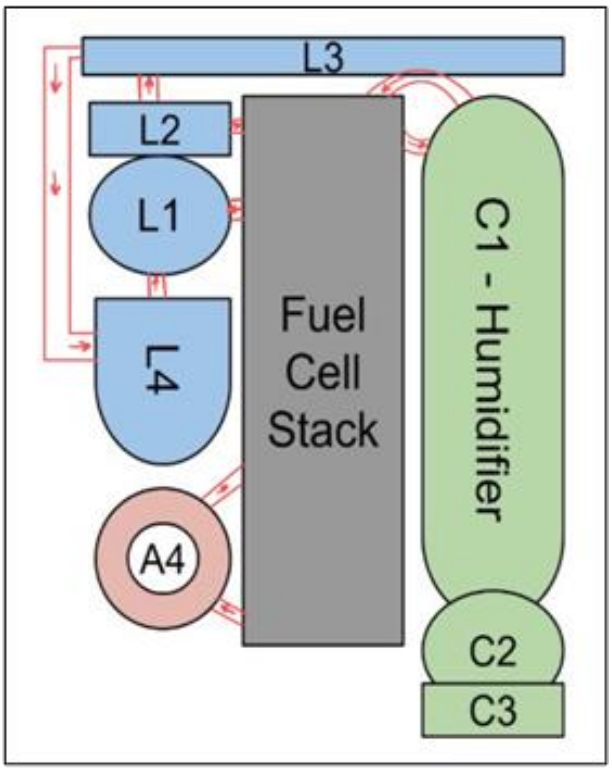

Figure 15: 2D model of optimized design layout of fuel cell system.

Once finalized, the 2D configuration was converted into a 3D CAD model, as displayed in Figure 16. This original CAD configuration allowed the team to visualize how the components would fit together and discuss ways to make the design more compact.

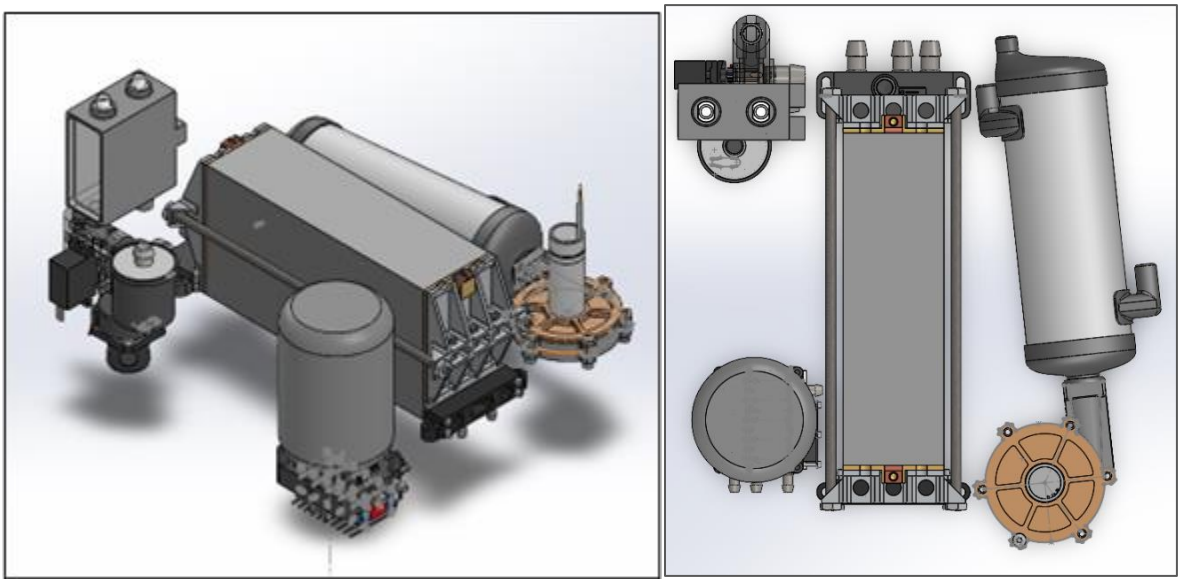

Figure 16: 3D CAD model of optimal design layout in isometric view (left) and top view (right).

4.3 Initial Design Concept

At this stage in the design process, we have understood the fuel cell system and have created a rough layout for the locations of each component around the fuel cell stack. We then developed a plan for producing a manifold design that takes advantage of effective manufacturing techniques while minimizing assembly labor. We came up with two ideas for the concept of the design.

The first idea was to utilize a pause-print technique to insert external components like the heat exchanger and humidifier into the manifold as it prints. It will be important to ensure there is a tight seal between the components and the manifold. This would require research into sealants or gaskets that will create an effective connection between the nylon of the 3D-printing and the material of the added part.

The second idea is to create one manifold that is split into two halves. This will allow external parts to be sandwiched between the two halves of the manifold. The separate halves will be 3D-printed, and the external parts will be inserted afterwards. Once the external parts are laid out into one half of the manifold, an identical half will be laid over the first half. This will require sealants or gaskets that ensure a tight connection between the two halves and the external parts and a sealant or fasteners.

The design utilized the latter “sandwich” idea for printing and assembling the system. Two manifolds would be designed and 3D-printed. External components including the humidifier and fuel cell stack would then be inserted between the manifolds and properly sealed.

4.4 Coolant and Cathode Manifold

The initial phase of the optimized manifold design started with determining component compatibility and strategizing their arrangement to maximize space efficiency and minimize pressure loss. We started with the coolant and cathode manifold, which manages the intake for both the coolant and cathode loops.

4.4.1 Original Design

The original manifold design was straightforward, consisting primarily of barbs that linked the fuel cell stack to tubing extending to various system components. Honeywell's initial manifold configuration is shown in Figure 17 below.

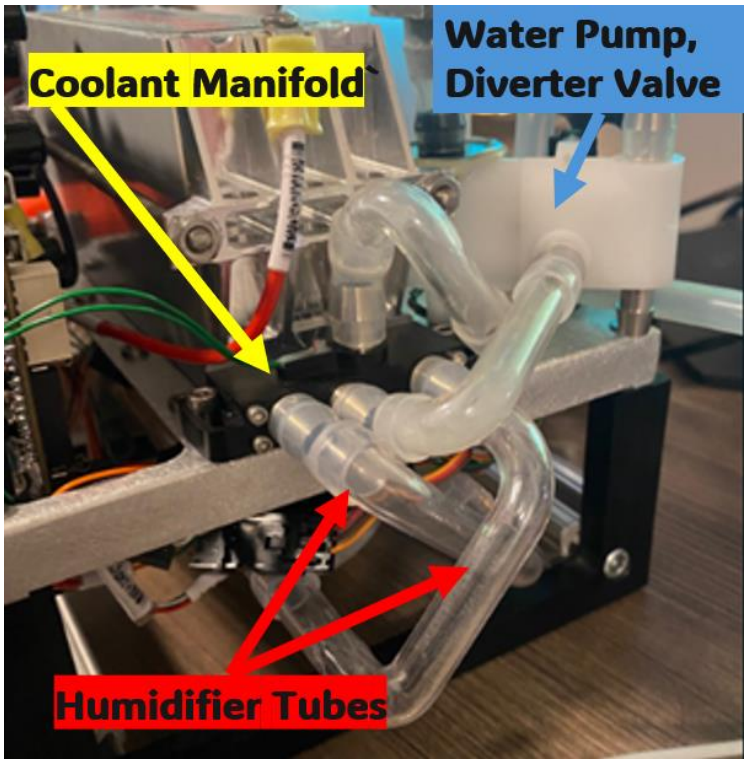

Figure 17: Original manifold assembly connecting water pump and humidifier to fuel cell stack.

Figure 17 depicts the interconnections among the fuel cell stack, original manifold, and tubing leading to other system components. The tubing arrangement was extremely chaotic, featuring numerous bends that increased pressure loss and added unnecessary weight to the system. Additionally, the water pump was haphazardly positioned beside the stack, and the humidifier was positioned beneath the stack. This configuration required multiple screws and additional hardware for mounting to the baseplate. Moreover, assembly demanded the manipulation and positioning of four distinct plastic tubes by the end-user, further complicating the process. In summary, this design was cumbersome, demanding extensive components and expertise for proper assembly.

4.4.2 Coolant Manifold Iteration 1

In our initial iteration, we directed our attention to the water pump, aiming to minimize the componentry linking it to the manifold. While preserving the foundational geometry of the original manifold (Figure 18), our design introduced enhanced pathway configurations.

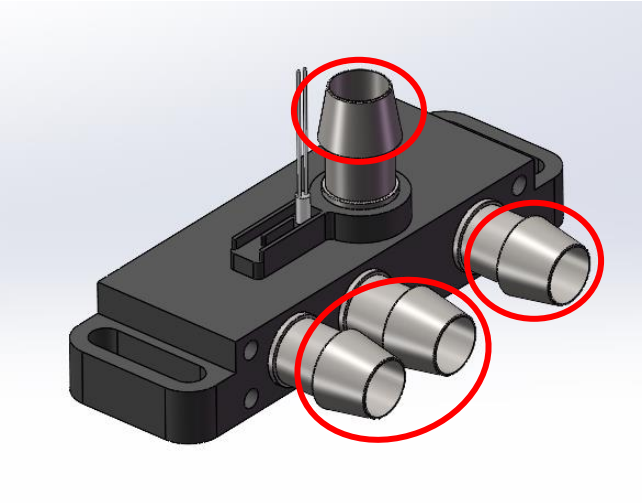

Figure 18: Honeywell's original water pump manifold.

The original manifold incorporated several barbs (circled in red) that linked various components to the fuel cell stack. Our initial design modification involved eliminating these barbs to remove the necessity for plastic tubing. Figure 19 showcases the first iteration of the coolant manifold, while Figure 20 presents the manifold seamlessly integrated onto the fuel cell stack, outlined in red.

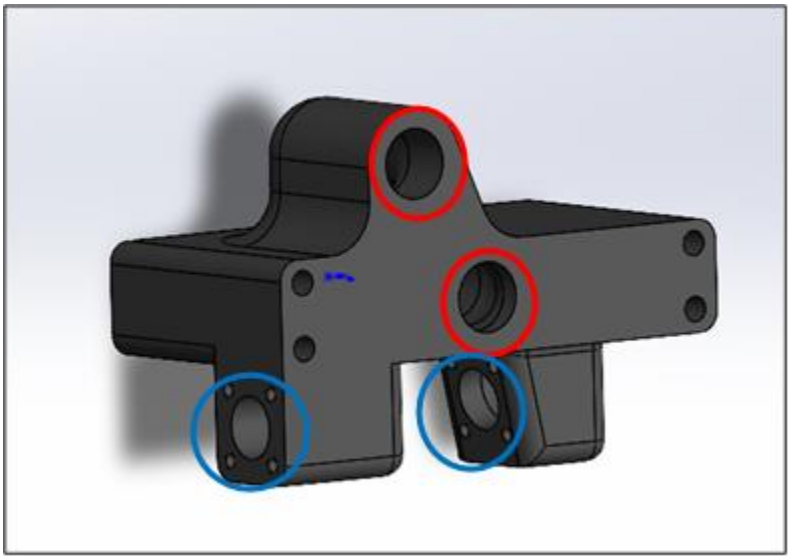

Figure 19: Iteration 1 of the coolant and cathode manifold.

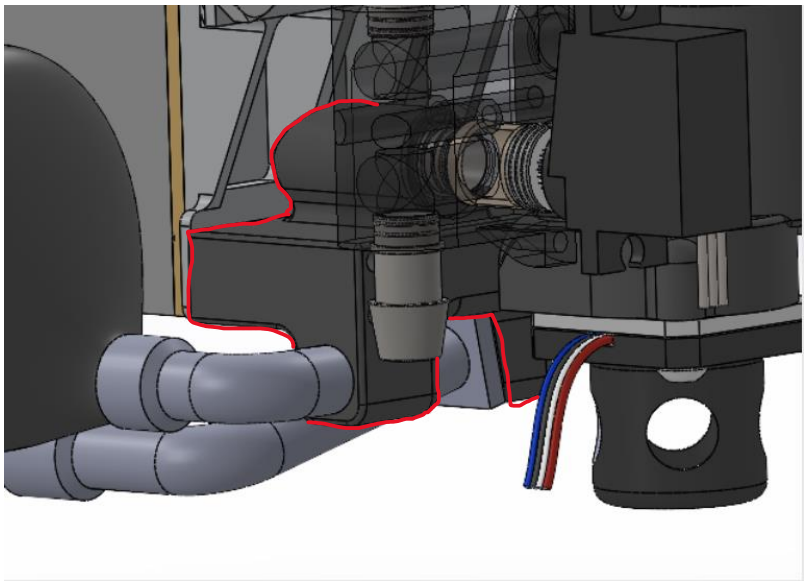

Figure 20: Iteration 1 of the coolant and cathode manifold attached to the fuel cell stack.

Looking at Figure 19, the front pair of holes is where the water pump attaches to the manifold (red circles) and the humidifier is connected via 3D printed tubing to the bottom pair (blue circles). Figure 20 shows the assembly of this configuration. The water pump interfaces directly with the manifold, eliminating the need for screws or additional tubing during assembly. Nonetheless, the assembly of the humidifier tubing necessitated further refinement, which we addressed in subsequent iterations.

4.4.3 Coolant Manifold Iteration 2

To improve upon our first iteration, we decided to incorporate the water pump housing, bypass valve housing, and the humidifier pathways into the design to be printed as a single part. We also created our own barbs on the bypass valve, removing the need to press fit the barbs. Figure 21 shows the second iteration of the coolant manifold with all the incorporated changes.

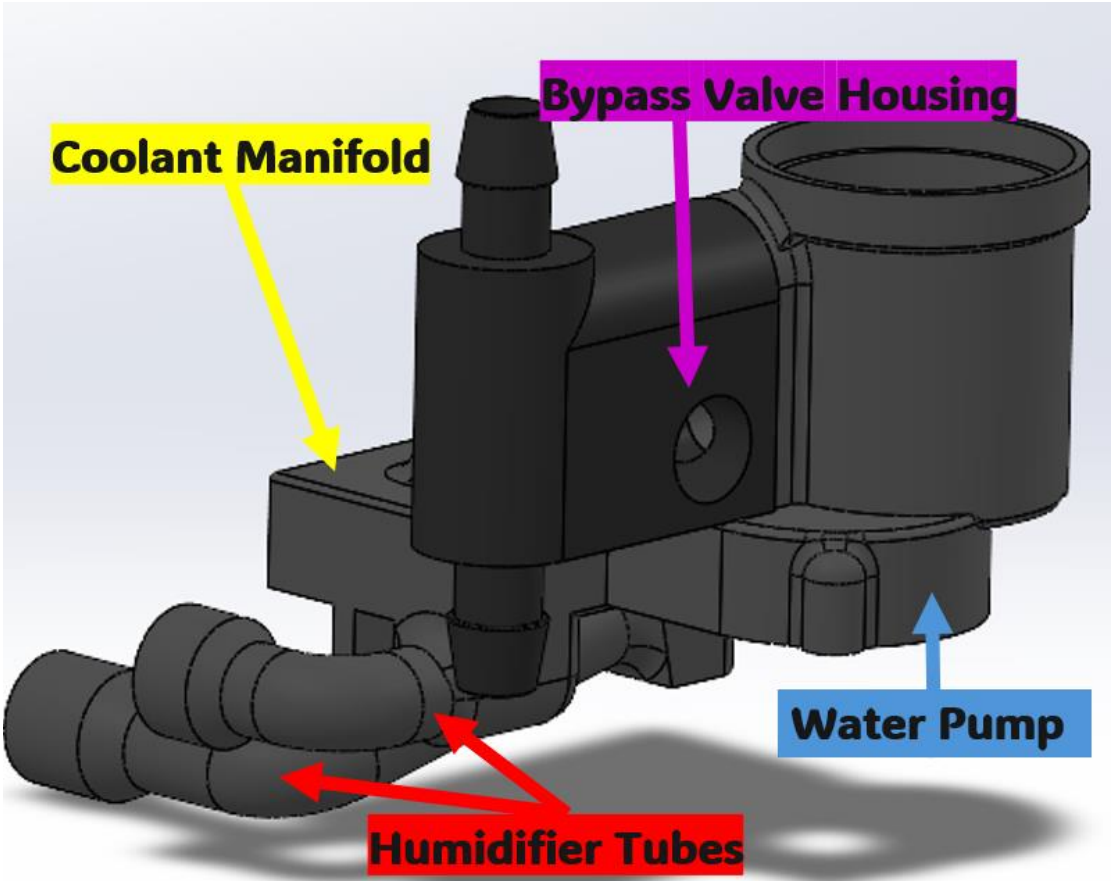

Figure 21: Iteration 2 of the coolant manifold.

As depicted in Figure 21, the water pump is fixed to the front pair of holes, while the humidifier is connected to the bottom pair. In this configuration, the water pump interfaces directly with the manifold, eliminating the need for screws or additional tubing during assembly. Nonetheless, the assembly of the humidifier tubing necessitated further refinement, which we addressed in subsequent iterations.

4.4.4 Coolant Manifold Iteration 3

In the second iteration, our focus shifted towards integrating components to enable their fabrication as a single unified part. Upon successfully 3D printing the second of the design, we recognized the potential to produce all plastic components as a cohesive unit, eliminating the necessity for tubes, seals, or interconnections between individual parts.

We positioned the water reservoir directly atop the water pump. In the existing design, the reservoir is connected to the pump with plastic tubing. Identifying an opportunity for further

streamlining, we combined the reservoir with the pump, thereby eliminating yet another connection. Figure 22 accentuates the reservoir positioned directly above the pump housing.

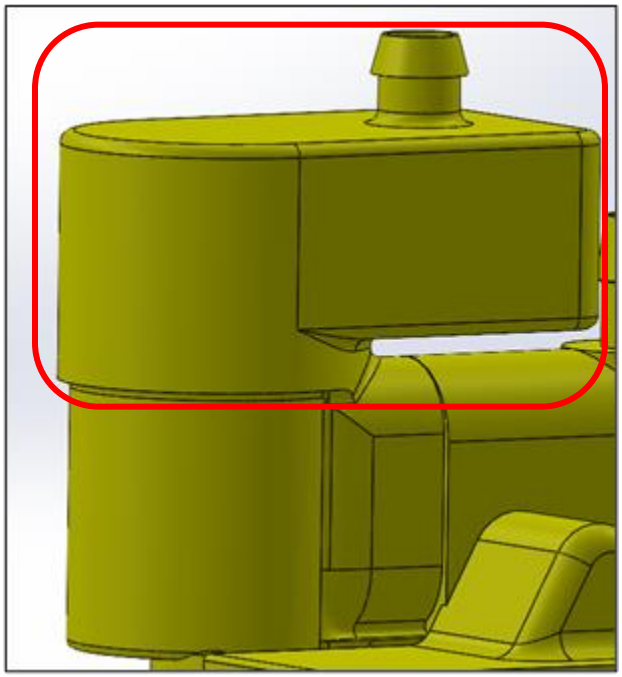

Figure 22: Water reservoir (outlined in red) added to the top of the pump housing.

Our subsequent design refinement involved incorporating mounting tabs for the bypass valve. Initially, the bypass valve was vertically attached to the bypass valve housing and required additional plastic tabs to be screwed into the housing. Once the plastic tabs were attached, the bypass valve was fastened to the tabs with metal screws. To reduce hardware, we integrated the mounting tabs directly onto the bypass valve housing, eliminating the need for separate plastic screw tabs and excess screws. Additionally, we reoriented the bypass valve horizontally to optimize its fit within the design, ensuring ample clearance for the screws. Figure 23 showcases the integrated tabs within the manifold.

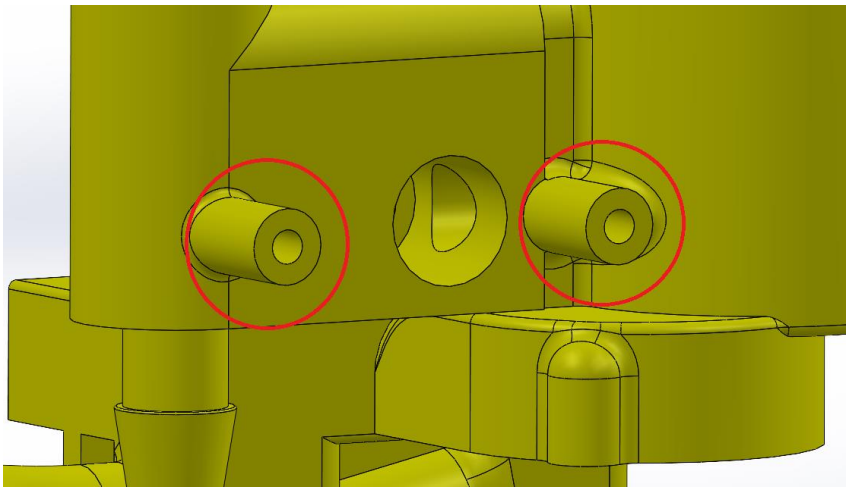

Figure 23: Mounting tabs for bypass valve built into the manifold (circled in red).

In the final adjustment of the third iteration, we integrated the humidifier cap directly onto the manifold. Previous iterations featured the manifold connecting to the cap, necessitating the use of O-rings, and demanding tight tolerance fits. To negate the complexity introduced by additional parts and potential tolerancing challenges, we incorporated the cap seamlessly into the manifold design. Figure 24 illustrates the humidifier cap integrated with the manifold.

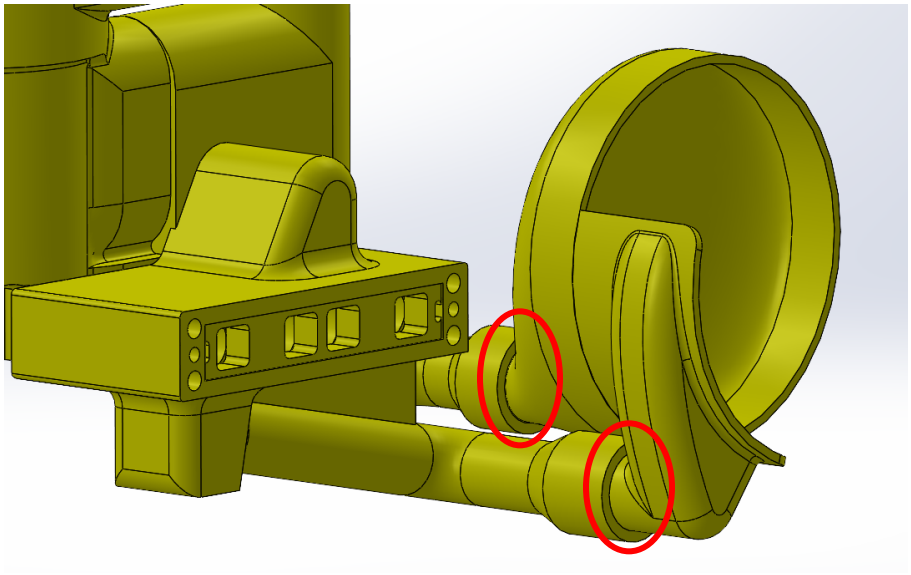

Figure 24: Humidifier cap built into iteration 3 manifold.

Following the refinements made in the third iteration, a few components still required separate assembly due to their mechanical nature, making it unfeasible to consolidate them into a single printed part. These components included the water pump, bypass valve, and humidifier.

In the original design, the water pump and bypass valve necessitated the use of two distinct screw types for mounting, presenting a challenge we aimed to address. The initial design incorporated both metric and imperial screws with varying head configurations. To streamline assembly and standardize screw types, we reengineered the water pump and bypass valve to interface with the manifold using universally compatible M3x10 screws.

Additionally, we transitioned to self-tapping screws, eliminating the need for customers to thread the screw holes during assembly. This adjustment not only simplified the assembly process but also enhanced user convenience. Figure 25 provides a comprehensive view of the final iteration in relation to the fuel cell stack and associated components.

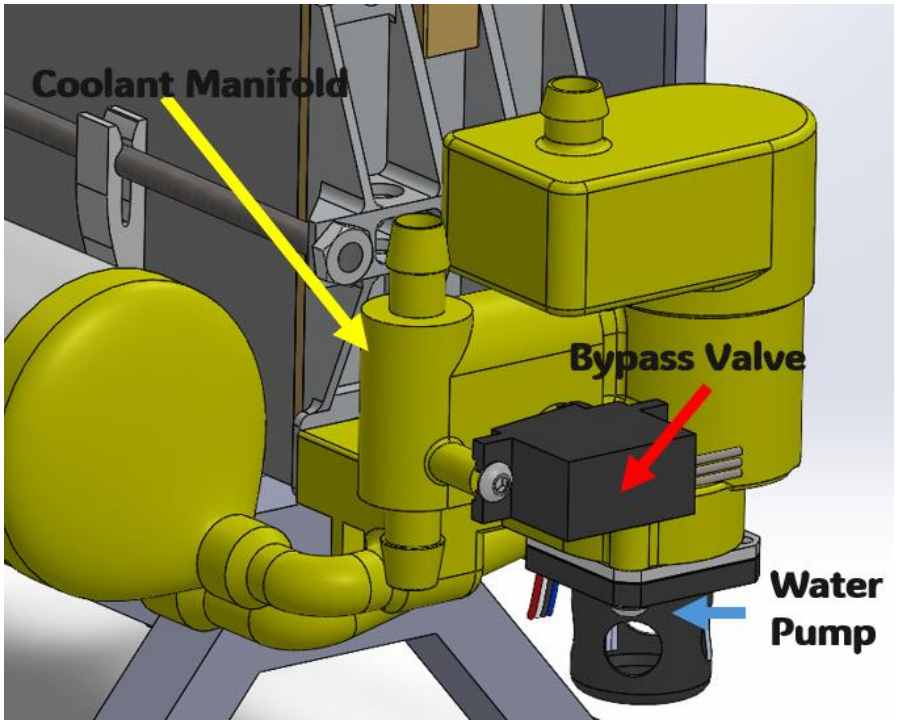

Figure 25: Iteration 3 manifold assembled onto fuel cell stack.

4.5 Blower and Ballast Manifold

After the original iteration of the coolant manifold was created, the team looked at the CAD model to determine which other components could be combined into a manifold. We determined that the ballast volume, solenoid valve mounting plate, the solenoid valves themselves, the cathode loop blower, and fuel cell stack mounting plate could all be combined into one manifold. Like the coolant and cathode manifold, the first step in designing the blower and ballast manifold was to understand how the system operates.

4.5.1 Original Design

Like the components that made up the original coolant loop, the components in the solenoid valve-to-ballast system and cathode air blower were seemingly pieced together with many pathways and different connection points (Figure 26). While there were less concerns over pressure loss for the anode loop due to the adequate pressure out of the hydrogen tank, the primary task was to minimize or eliminate pathways between the solenoid valves and the rest of the connection points.

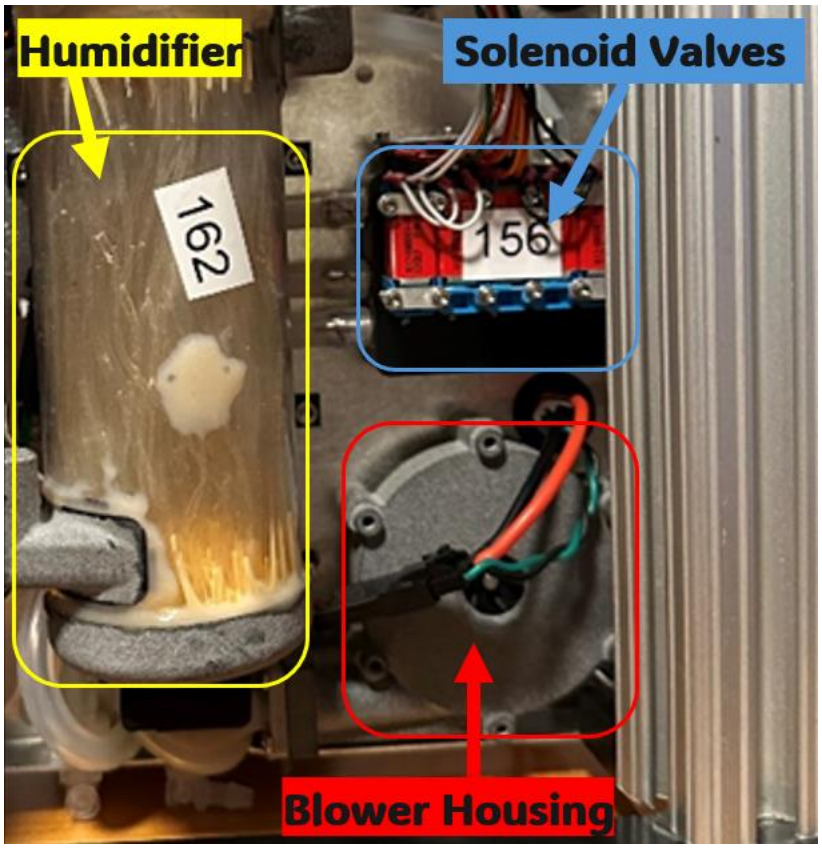

Figure 26: Initial mounting plate for the air blower, humidifier, and solenoid valve subassembly.

4.5.3 Blower Manifold Iteration 1

It was clear that some parts would need adjusting before being combined into a single part. We knew that we could leverage additive manufacturing to incorporate the ballast volume into any open space within the manifold, so we saved this for last. We sought to eliminate the tubing pathways from the solenoid valves by attaching the solenoid housing directly to the fuel

cell stack. Also, we determined that the air blower housing piece, end cap, and exhaust port could be combined into one part.

The first manifold iteration focused on connecting the solenoid valve plate with the fuel cell stack mounting plate (Figure 27). This involved creating new internal pathways which would be easily manufactured with the multi-jet process. This preliminary task determined the available geometry for the rest of the design. Although seemingly simple, this task was important because we needed to maintain the existing mounting geometry for attaching the manifold to the fuel cell stack, and we had to consider ways to physically assemble the manufactured part with other components.

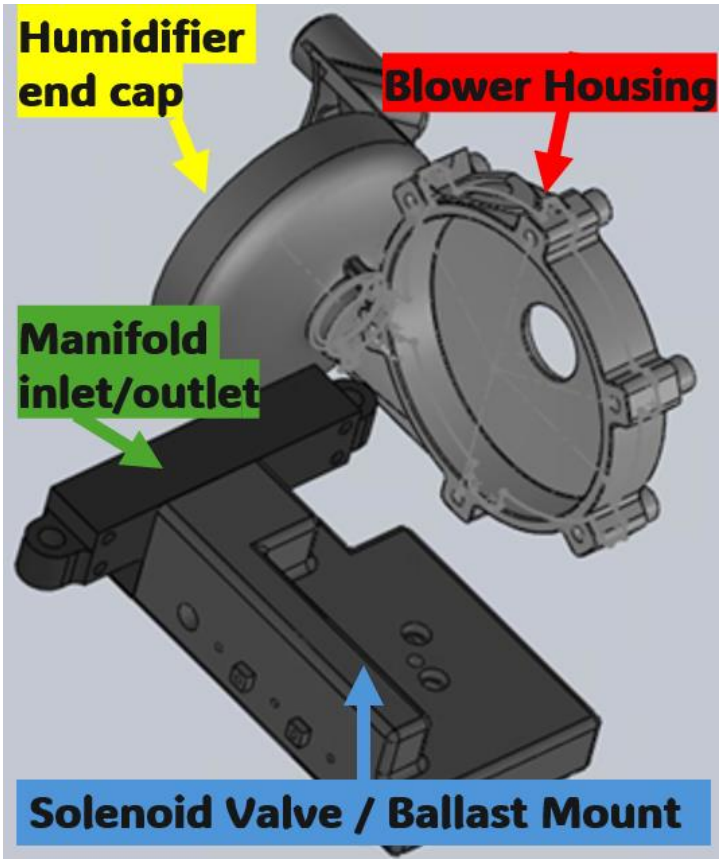

Figure 27: Iteration 1 of the blower and ballast manifold.

4.5.4 Blower Manifold Iteration 2

After a prototype print of the first manifold iteration in FDM, the team continued with the design vision. We added a ballast volume to the part, which we calculated to hold roughly 2.5 ounces. The blower mounting plate was also connected to an extended surface of the geometry

created in the first manifold iteration. We then attached and combined the end cap and exhaust port part onto the blower mounting plate.

Lastly, the team researched an activated charcoal filter for the air blower and integrated housing into the manifold. An air filter was necessary to prevent small particles from entering the cathode loop and interfering with the flow of oxygen into the fuel cell stack. Activated charcoal was selected as a desirable air filter material due to its ability to filter out volatile organic compounds (VOCs) which would impact the performance of the fuel cell system over time. The second iteration is shown in Figure 28 below.

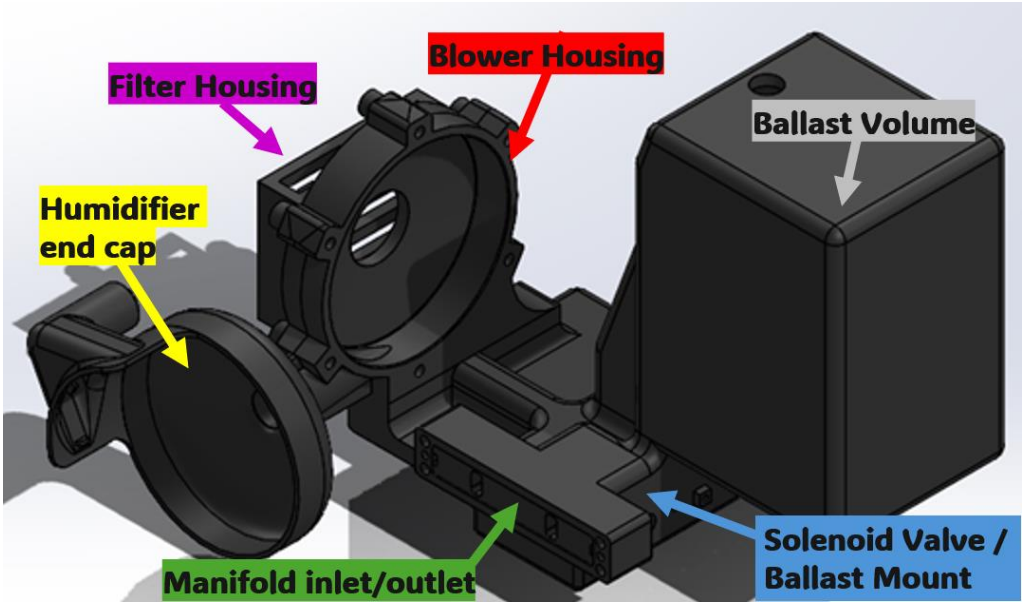

Figure 28: Iteration 2 of the blower/ballast manifold.

4.5.5 Blower Manifold Iteration 3

After completing a visual design review of the second iteration of the blower and ballast manifold, the team identified key areas to focus additional work on. First, we found that the ballast volume exceeded the maximum extent volume of all other components and required spatial adjustment. To account for this, the team moved the ballast volume to conform around the fuel cell stack, but still within the maximum extent volume possible. The existing design for the blower mounting plate used tapped holes; however, the team determined that self-tapping screws would be ideal in this use case. The 6 holes on the blower mounting plate were accordingly sized to 2.5 millimeters to accept the M3 self-tapping screw which will be used to attach the blower. Once the second iteration of the blower and ballast manifold was placed in a full assembly, the

team realized the exhaust port on the manifold was slightly misaligned with the opening in the humidifier. The team easily adjusted the exhaust port placement to properly fit with the humidifier opening. Barbs were also added that secured tubing to the manifold for the ballast exhaust pathways and for connecting the system to the hydrogen tank. The third and final iteration of the blower and ballast manifold is shown in Figure 29.

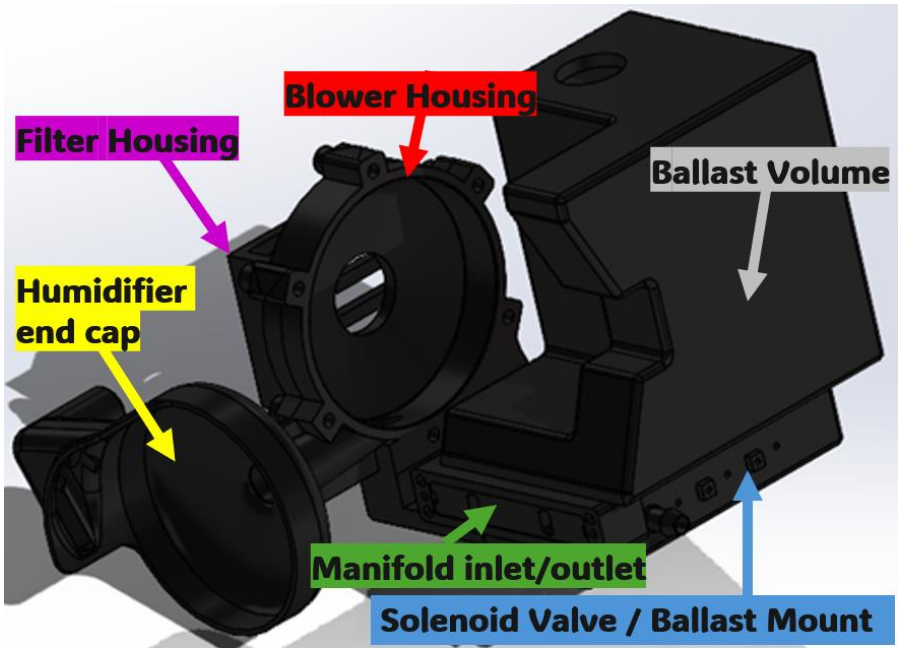

Figure 29: Iteration 3 of the blower/ballast manifold.

In addition to conceptual design changes, the team also analyzed the manufacturability of the design. Based on a preliminary part manufactured by Sicam, the team identified areas of concern for this manifold. A hole was placed on the top of the ballast, intended to ease the removal of loose nylon particles from the ballast volume and internal hydrogen "straws." Two additional ports to aid in the nylon particle removal process were added to the complex internal pathways of the solenoid valve plate. These access ports feature plugs in the final assembly.

4.6 Additional Design Features

4.6.1 PCB Mounting Frame

Mounting the PCB board was one of the final steps in the design process. The team knew that we wanted to mount it using a snap feature to eliminate the need for any hardware and reduce the overall weight. After exploring the many types of snap joints, including cantilever,

torsion, U-shaped, annular, and interlocking, we determined the optimal joint for the design of the PCB mounting frame would use an annular snap joint and cantilever snap joint. The electronic board has many extrusions at various heights, so creating a mounting plate was quickly eliminated from the options. Instead, we switched to the option of a mounting frame, which would hold the board around its perimeter, avoiding the boards extruding components.

The team decided that a mounting frame with cantilever snap joints on both sides and on the bottom would properly secure the board to the frame. The PCB board would be snapped in on the right and left sides with two snap hooks and on the bottom with one snap hook. An example of a snap hook is shown in Figure 30 below.

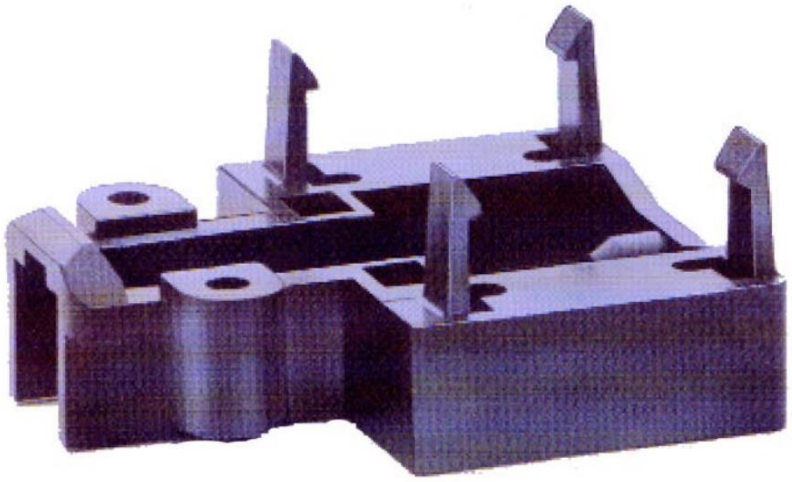

Figure 30: Example of a cantilever snap joint, as shown in the Bayer Material Science LLC Design Guide for Snap-Fit Joints for Plastics (n.d.).

After securing the board to the frame, we decided to connect the mounting frame to the screw connected to the fuel cell stack housing using an annular snap joint. This kind of joint is rotationally symmetrical and involves multiaxial stress. Usually, a circular hoop extends when pushed onto a rigid matching groove, causing stress to develop in the annular hoop, and generating frictional force to hold it on the grooved structure (MIT Fab Lab & Bayer MaterialScience LLC, n.d.). An example of this joint is depicted in Figure 31 below.

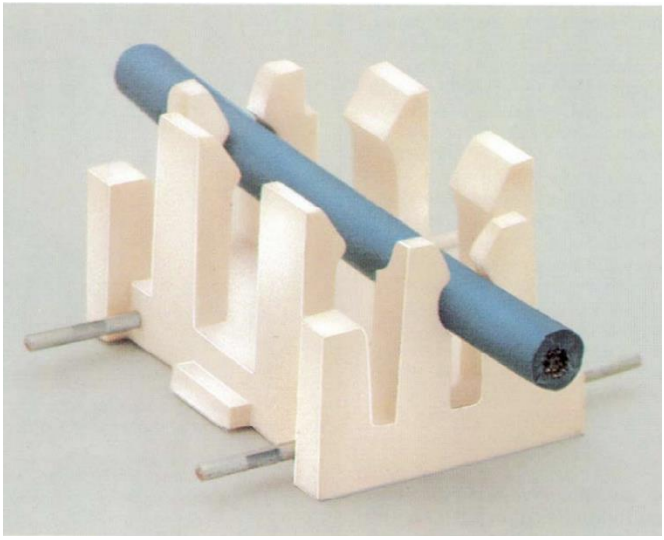

Figure 31: Example of an annular snap joint that was used to model the annular snap joint on the mounting frame, as seen in the Bayer Material Science LLC Design Guide for Snap-Fit Joints for Plastics (n.d.).

The first iteration design with the snap hooks and the annular snap joint is displayed in Figure 32. This design displays four annular snap joints coming off the back of the mounting frame. The annular snap joints were designed based on the radius of the lead screw on the fuel cell stack, and the number of connections that would be needed to secure the board. The team also added a support bar underneath these snap joints to keep the mounting frame from rotating about the x-axis. Then, we added a rectangular extrusion on two corners diagonal from each other to ensure that the PCB board would not fall backwards.

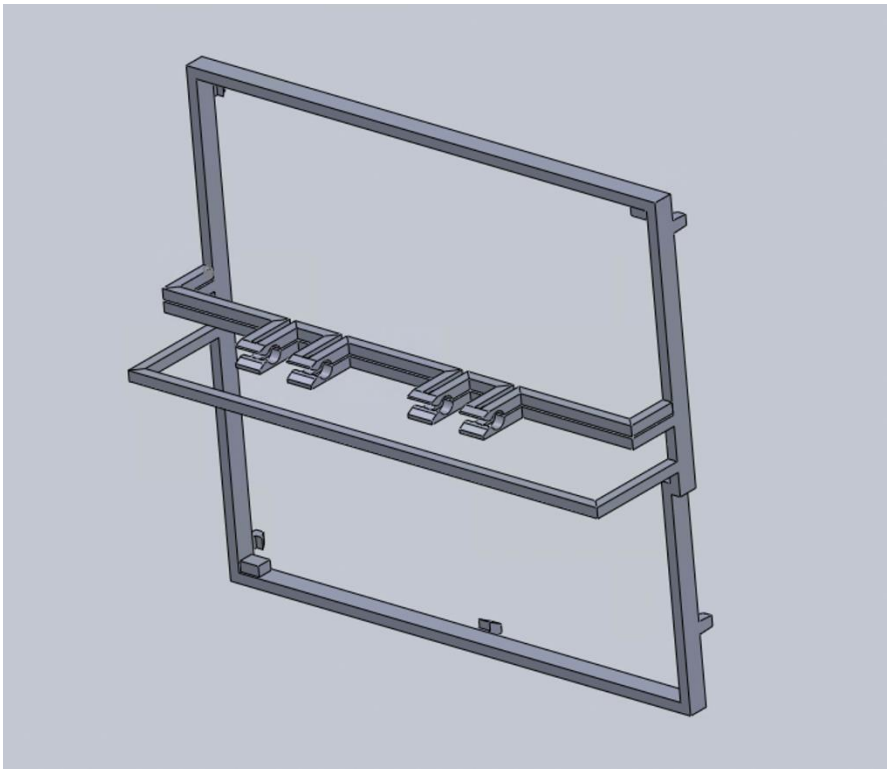

Figure 32: First iteration of PCB Mounting Frame design in CAD space.

The team printed this frame design using resin 3D printers to conduct initial fit tests and see if the frame would properly hold the board and attach to the fuel cell stack. The PCB board snapped into the frame and held nicely. However, we quickly found that the annular snap joint parts of the frame were not strong enough to hold to the fuel cell stack. Therefore, we eliminated the gap between the top and bottom of the joints and strengthened it by adding material to the round pieces of the joints. The second and final iteration is shown in Figure 33 below. This image depicts these thicker snap joint pieces and the thickened arms holding them. The team also decided to add material to each of the four corners of the frame for additional support.

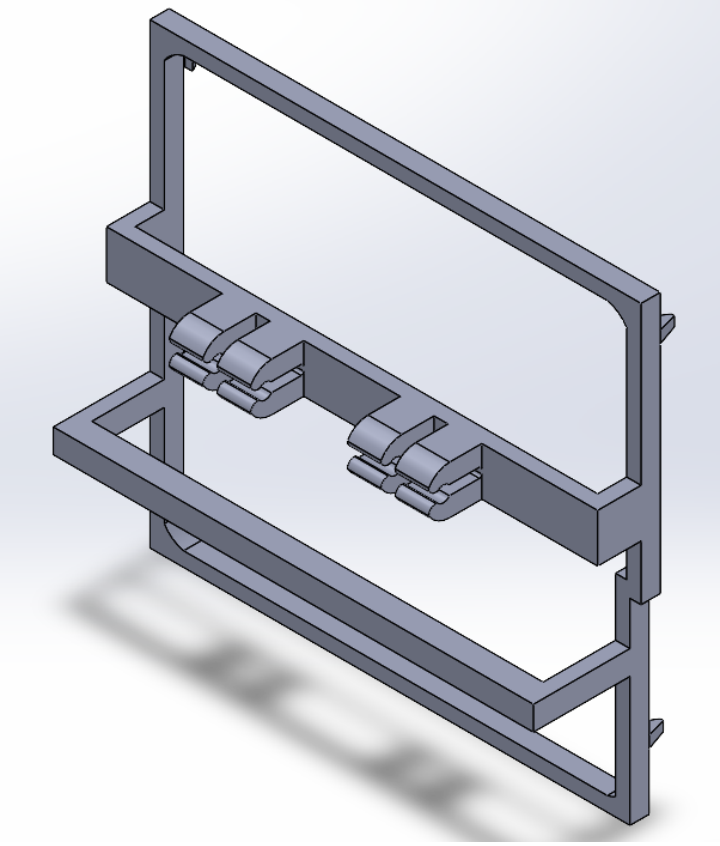

Figure 33: Final PCB Mounting Frame design in CAD space.

After this second iteration, we 3D printed the frame with resin again and found it held the PCB board and was able to properly attach and hold to the fuel cell stack. The design of the PCB board demonstrates the functionality and feasibility of snap joints to avoid extra hardware while still properly securing components in a design. In this case, the PCB board will be much easier to attach to the fuel cell than before, making it easier to assemble.

4.6.2 Support Stand

The support stand was created for structural and aesthetic purposes. The stand was a necessary component to design and manufacture because the system cannot sit flat due to the manifolds abutting asymmetrically. The stand allows the fuel cell system to suspend flat, a few inches from the ground or table it rests on. The stand also offers aesthetic appeal by raising the system above the surface it is placed on (Figure 34).

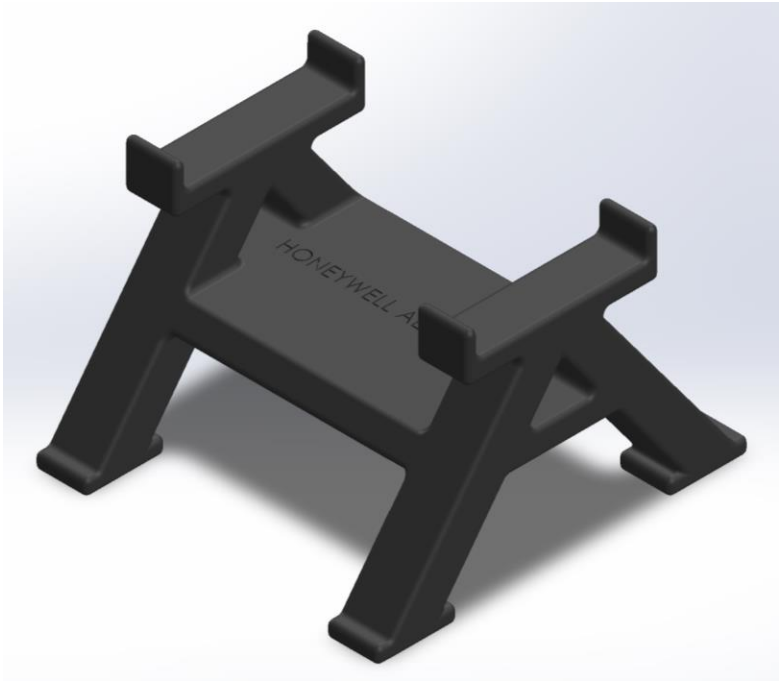

Figure 34: CAD model of system support stand.

The design of the stand itself also features aesthetic aspects. The letters “H” and “A” can be read from the side and front planes, respectively, representing the sponsor of this project, Honeywell Aerospace. The word, “Honeywell Aerospace” is also engraved along the top plane of the stand’s structural beam.

4.7 Final Design of Entire System

Throughout the entire design process, the team kept our design objectives in the front of our minds. We ensured that making the design as compact and lightweight as possible, while reducing part count and ease of assembly were priorities. After each iteration, we analyzed the design together, determining what can be improved and how, and improving on the design as much as possible for the next iteration.

Once the design of both manifolds and supporting pieces were complete, the group assembled all components into a SolidWorks assembly file to ensure that everything was dimensioned correctly. In the assembly file, everything mated and meshed well, giving it a sleek look and reassurance that our physical model will work. Figures 35, 36, and 37 display this entire assembly with both manifolds, the PCB mounting frame, and the support stand. The Bill of Materials for this optimized design can be found in Appendix III.

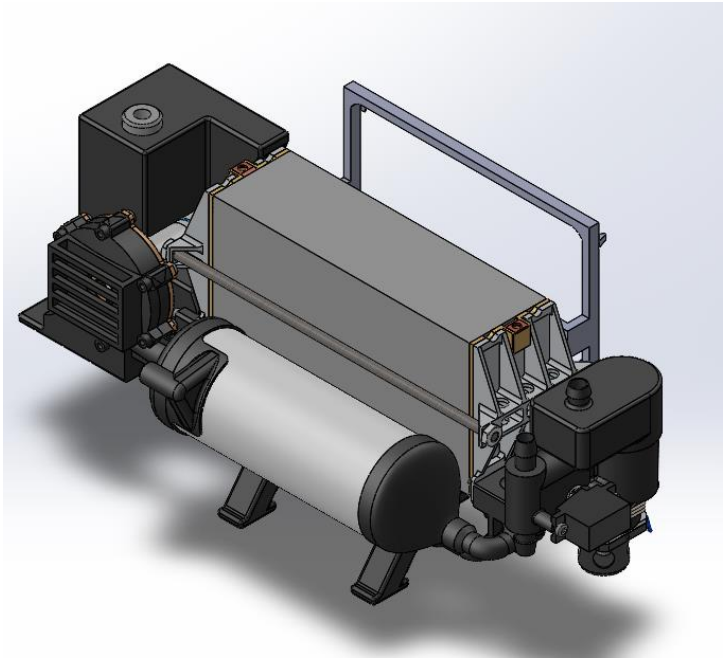

Figure 35: Isometric view of the entire fuel cell assembly in CAD.

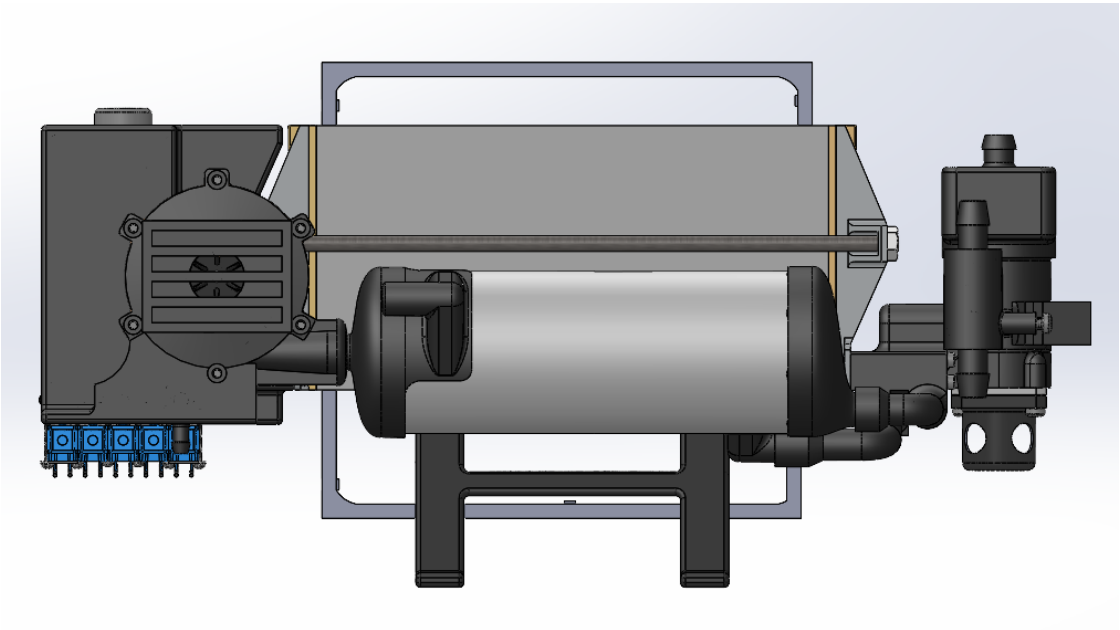

Figure 36: Side view of the entire fuel cell assembly in CAD.

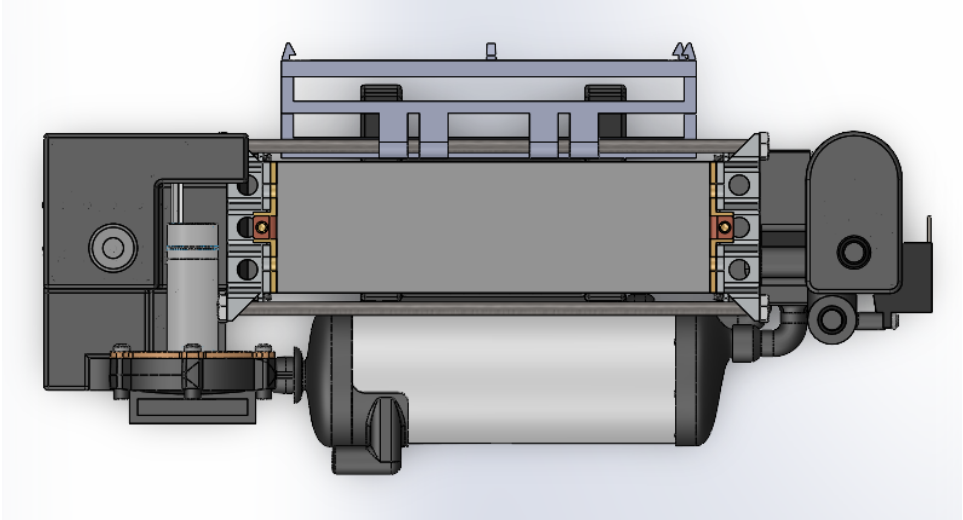

Figure 37: Top view of the entire fuel cell assembly in CAD.

4. Results and Analysis

The goal of this project was to design a fluid and gas distribution apparatus for a PEM fuel cell system by exchanging components and altering pathway configurations to minimize power losses, weight, and volume while maintaining reliability and long-range capabilities. In order to properly verify our design, the team conducted several tests. First, we examined how the manifold pieces fit when assembled onto the whole fuel cell system and observed any tolerancing issues. Then, we conducted hydrostatic pressure testing to investigate if there were only liquid or gas leaks in the manifold pieces. Finally, full testing was conducted in the lab and power output and gross power were recorded.

5.1 Geometric Fit Tests

After the manifold designs were finalized, they were 3D printed using nylon multi jet printing at Sicam, and the PCB board and support stand were printed using resin 3D printers. Once printed parts were obtained, our team tested for initial geometric fits and noted any components that had fit issues.

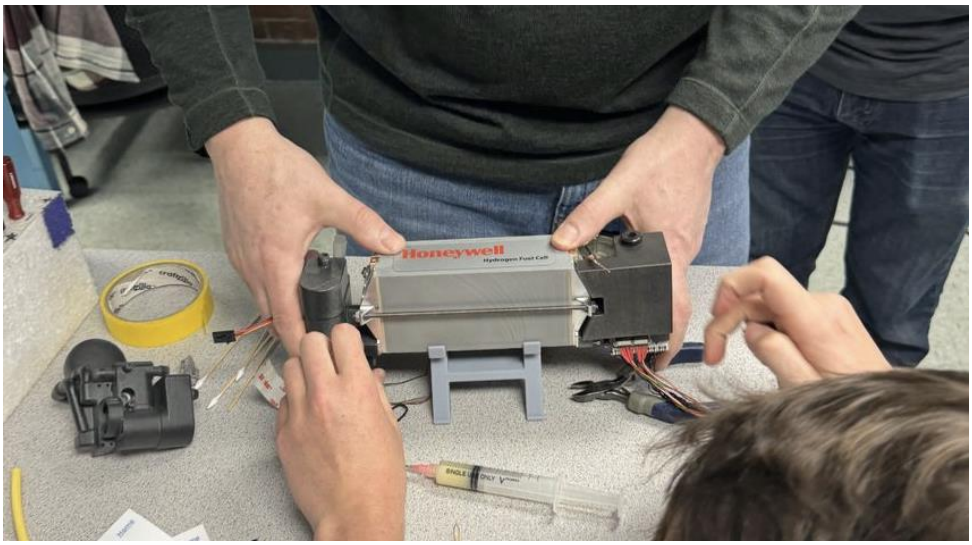

Figure 38: Geometric fit tests for coolant manifold and blower/ballast manifold.

The initial print of the coolant/cathode manifold appeared to be mostly successful in terms of fit. The humidifier fit perfectly into the humidifier cap and the pump fit well in the pump housing. One slight adjustment we needed to make was to increase the diameter of the circular insert for the pump O-ring, to ensure that the ring would fit. Another adjustment we had to make to the part was reaming out the hole for the bypass valve to 3/8in. To ream the part, we

clamped the manifold in a vice grip and inserted the reamer vertically and began to ream the hole to 3/8 inches. This set up can be seen in Figure 39.

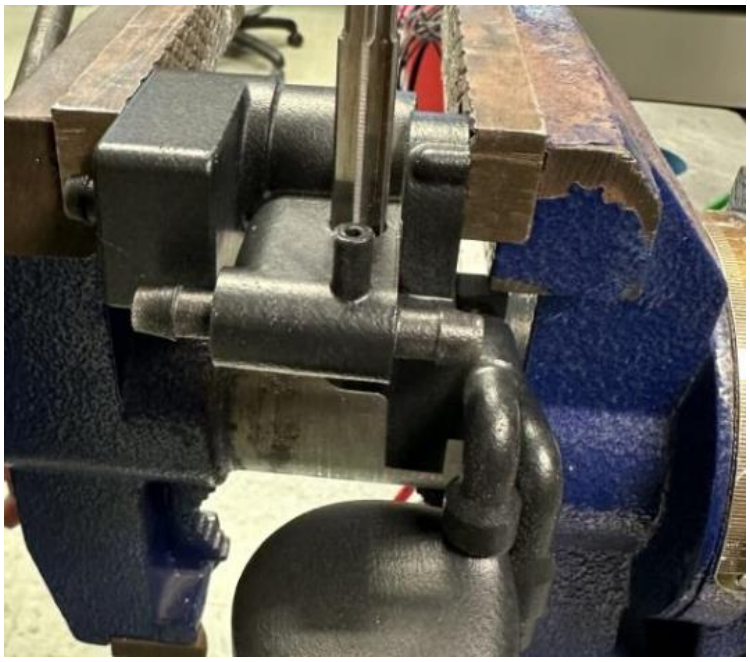

Figure 39: Setup to ream the hole for the bypass valve in the coolant manifold.

We purposely made this hole smaller so we could achieve a perfect diameter with the reamer and avoid tolerancing issues in the 3D printed part.

Like the coolant/cathode manifold initial print, the blower/ballast manifold fit test went well. Once again, the humidifier fit well into the end of the cap. A minor change was made to have the pump gasket attachment piece attached as an extrusion, rather than as a circular indent, to ensure it would fit properly and account for tolerancing issues.

The team used these initial prints and fit checks to ensure that the design was printed properly, and everything was sized correctly. As a result, we made minor changes needed to ensure everything would fit well and made our design more reliable.

5.2 Hydrostatic Pressure Testing and Adjustments

To test the coolant manifold, we had to create a test environment in which the water pump was the only working part. To run the test, we attached the manifold to one end of the fuel cell. Then, to cap the other end of the fuel cell, we attached the original anode manifold that

would seal the water channels on that end. Once we attached both pieces to the manifold, we connected the pump to a power supply unit and set it to 12 volts. The testing set up can be seen in Figure 40 below.

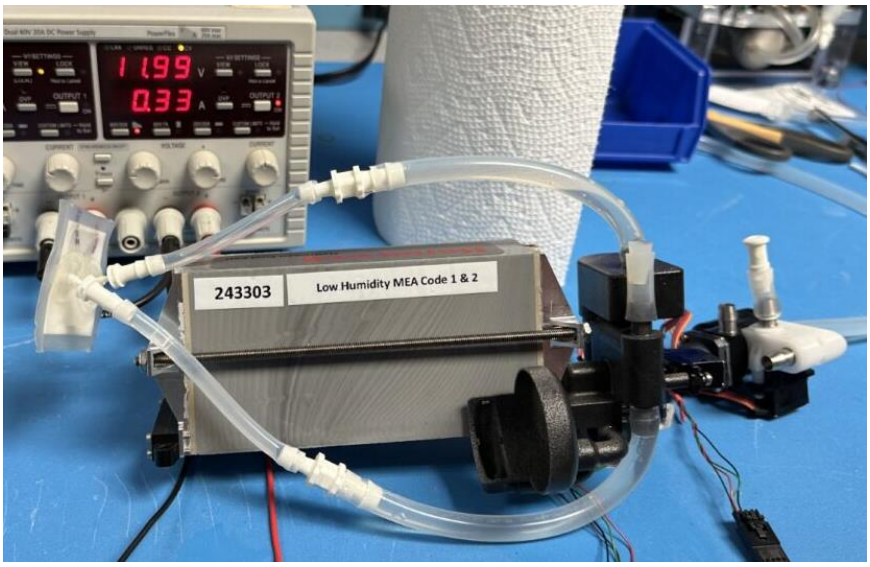

Figure 40: Testing setup for the coolant manifold.

Once those parts were set in place we began priming the pump. We turned the pump on and off, continuously filling it up with water as more air bubbles were pushed out of the system. To find leaked areas, we set paper towels underneath to identify the locations of any significant leaks.

In our initial run the water was able to smoothly flow throughout the manifold and the fuel cell once all the air bubbles were purged from the system. We did notice that the manifold was leaking in several places. More specifically, the attachment site between the coolant manifold and the fuel cell, the bypass valve, and the seal between the fuel cell and the original anode manifold. Without the ability to fix these surfacing issues at that moment, we resorted to a quick fix that would help minimize the leaking and be sufficient testing the whole system. We noticed that the screws on the bypass valve were not completely torqued down and that was why it may have been leaking, so we finished torquing these down and began looking to mitigate the sealing issues between the manifolds and the fuel cell. To fix these, we applied vacuum grease on the manifolds, fuel cell sealing surfaces, and the gaskets between the two parts. Once we applied these changes we began testing the system again.

In the system's second test, the mating surfaces between the fuel cells and the manifold were sealed, and there was no leaking in those areas. The bypass valve was still a little leaky, but not at the same rate as the first test. After the second test, we were happy with the results and concluded that the coolant manifold was ready for use in the full system test.

To test the anode loop, the team used pressurized air at about 5 psi and inspected the assembly by applying soapy water to sealing connections. The team then operated the ballast purge system to ensure there were minimal leaks between the blower/ballast manifold and each solenoid valve. With a mass flow meter plumbed in-line with the compressed air source, the team recorded a value of 0.04 grams per second which was deemed acceptable by the engineering team at Honeywell to proceed with our full testing. The team identified critical leak areas around both fuel cell stack to manifold connections along with where all solenoid valves attach to the manifold.

To test the cathode loop of the system, the team wired the blower up to the PCB and ensured everything was working properly. One key difference between our system and the original system was the spin orientation of the blower, meaning for our test we had to reverse the polarity of the blower to get it to properly pressurize the internal cathode loop.

After the preliminary pressure testing with air, we initiated pressure testing with hydrogen in the Honeywell wet lab. During this test, we immediately encountered multiple leaks. Notably, leaks were coming from both attachment sites of the manifolds, where there are semicircular indents in the stack, and significant leakage from the solenoid valves. To address the solenoid valve leaks, we applied vacuum grease to both sides of the rubber gasket between each valve and the manifold. To tackle manifold leakage, we tightened all screws at the attachment sites. In our second test the leaks from the manifold attachment sites were significantly reduced, however the leakage from the solenoid valves worsened. We then opted to completely disassemble all solenoid valves, applying vacuum grease to each valve gasket individually to achieve a tighter seal. Also, clamps were fixed to the solenoid valves to create a better seal shown in Figure 41.

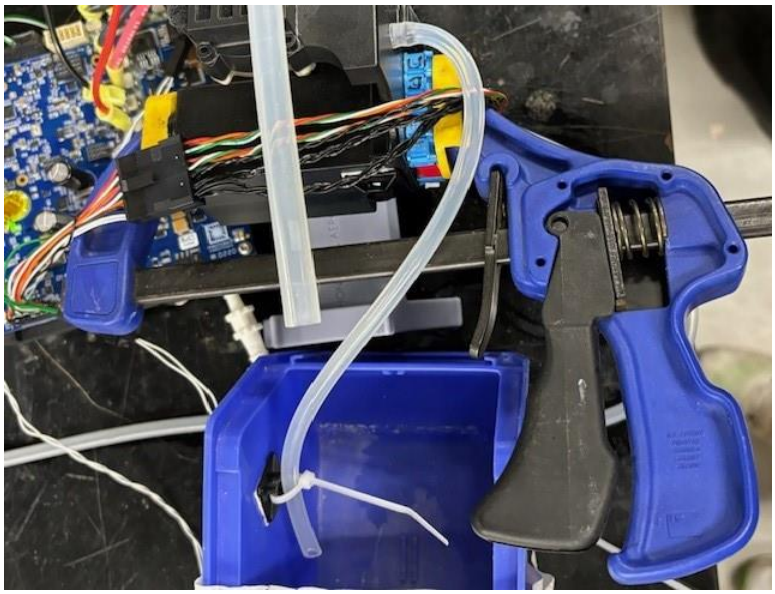

Figure 41: Clamp applying pressure to solenoid valves.

These measures resulted in less leakage, albeit some residual leakage persisted. However, these adjustments allowed us to proceed with comprehensive testing of the entire system.

5.3 Final Test Results

During the full testing of the fuel cell assembly, the sensors and PCB attached to the system recorded data which we analyzed afterwards. Figure 42 below shows the power output from our fuel cell system in the dark blue color. From the graph below, the warm-up phase of our test run can be seen in the first roughly 2000 seconds of the test. The team then adjusted the orientation of the assembly, as it was adjusted during the final sealing checks, before completing the test of the assembly. From this graph, the system produced roughly 450 watts on the 600-watt fuel cell stack assembly for over 11 minutes consecutively under the best operating conditions we achieved. The most typical operating conditions occurred between approximately 2600 seconds and 4000 seconds, during which time the ballast purge control system was operating properly.

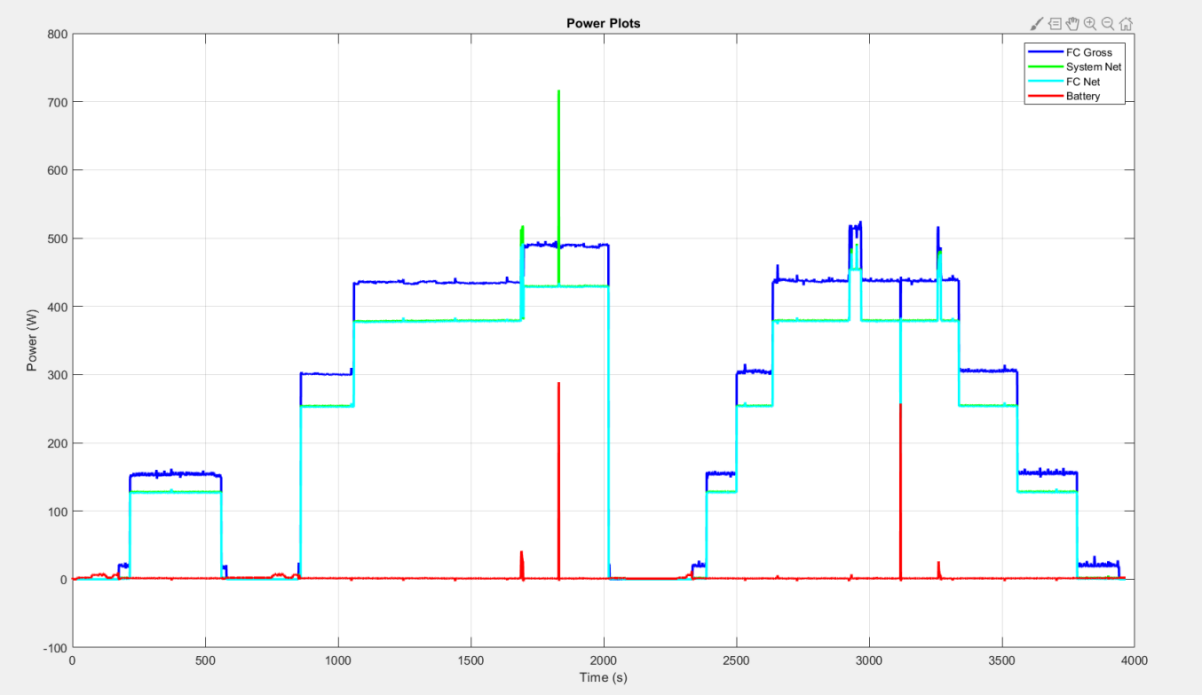

Figure 42: Power plots for the final testing of the full fuel cell assembly, with time in seconds on the x-axis and power in watts on the y-axis.

The team identified four main reasons why the gross power output was below the anticipated value of 600 watts:

1. The anode loop did not seal well enough to maintain adequate pressure which negatively impacted the voltage produced by the stack.
2. The leak in the anode loop resulted in the normal purge scheme failing to operate properly, meaning water flooded the anode loop and resulted in a negative impact to the voltage produced.
3. The bypass valve (component L2) was not able to actuate as the bypass valve body was angled differently than the original positioning which negatively impacted the voltage due to the stack running too hot or too cold at times.
4. The stack the team used for final testing and results had not been hydrated in a long time and would have produced more voltage if it was fully rehydrated; however, fully rehydrating the stack can take more time than we had available.

Despite the issues identified above, the results were extremely promising for our design. Not only was our assembly able to produce around 75% of the gross power expected under unideal conditions, but we were also able to almost perfectly match the nominal gross power produced

for a 600-watt stack assembly, as seen from Figure 43 below. Below an output current of 10 amps, our assembly almost perfectly matched the nominal value. As we attempted to increase the output current (and subsequently the gross output power) the sealing issues began to negatively impact the stack functionality, and thus the power output of the assembly.

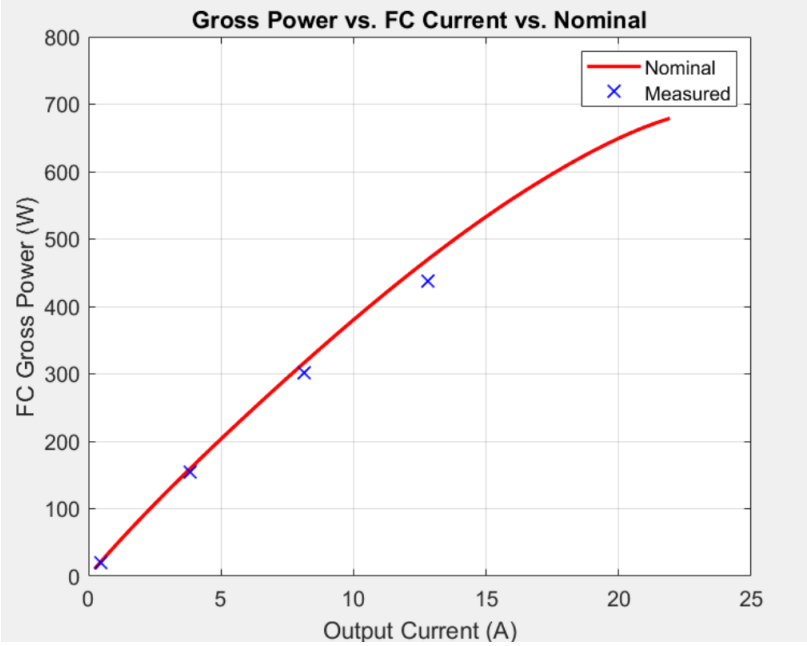

Figure 43: A graph highlighting nominal versus measured output current and gross power, with output current in amps on the x-axis and fuel cell gross power in watts on the y-axis.

In Figure 44 below, the ballast pressure and the output current can be seen in light blue and pink respectively. In the time before 2000 seconds, the fuel cell was still rehydrating, and the team was working to get the ballast purge control system properly operating. This translated into the first 2000 seconds of our test to produce power successfully, but without multiple different ideal operating conditions such as ballast pressure, ballast moisture content, and moisture content of air entering from the cathode side. Around 2300 seconds into the test, the system was operating much more typically which can be seen in the repetitive drops in the ballast pressure in the graph below. While intuition might suggest that higher pressure relates to a better power output, that is not the case. In the time after 2300 seconds, the most current produced occurred when the ballast pressure was around 10 psig. When the ballast pressure was raised to around 14 psig, the leaks in the anode loop prevented the control system from operating as expected, and thus the output current was greatly reduced (seen in the last “step” of the graph below).

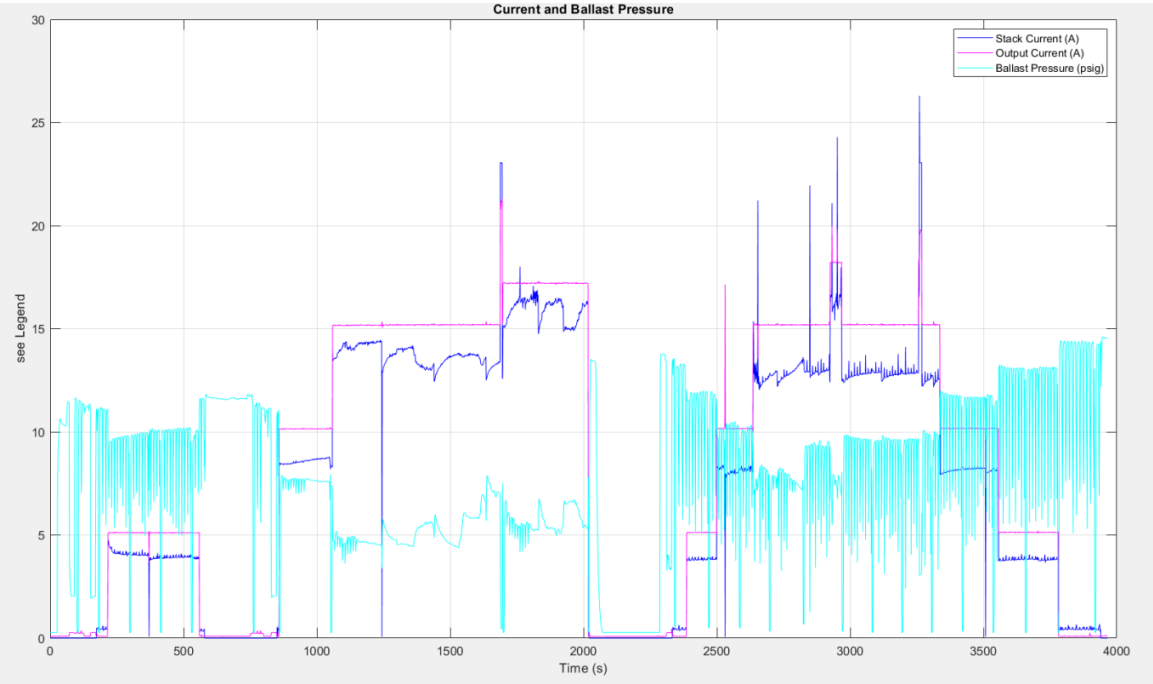

Figure 44: Current and ballast pressure for the for the final testing of the full fuel cell assembly.

5.4 Final Design Comparison

Reflecting upon our original design objectives, we redesigned the manifold to reduce part count, maximum extent volume, pathway lengths, and weight. A side-by-side comparison between the original and new designs are displayed in Figure 45 below.

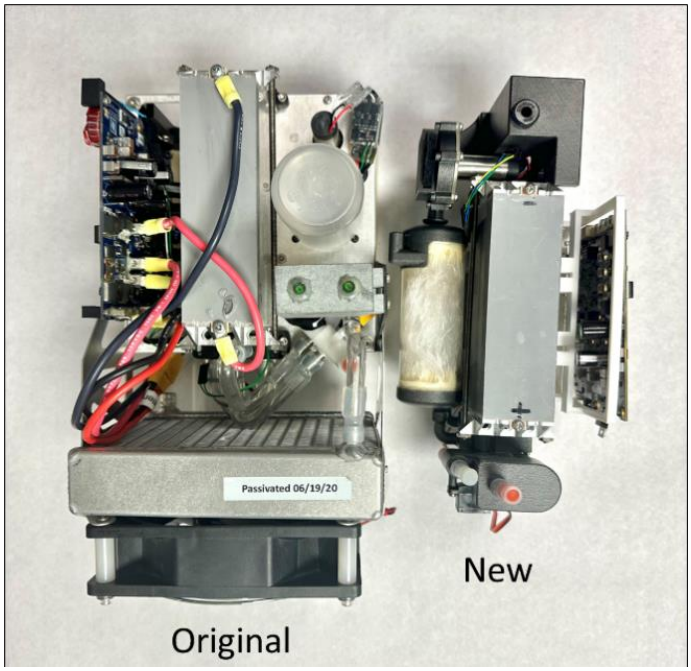

Figure 45: Side by side comparison of original and optimized fuel cell systems.

Using various design techniques and keeping design for manufacturability in mind, we successfully minimized the design complexity, resulting in a simpler assembly process. Additionally, we reduced the volume and weight by creating one manifold piece that can hold components for the coolant and cathode loops. With this new design, Honeywell can increase power efficiency, and customers can more easily assemble the system. The major areas of improvement are visualized in Figure 46 below.

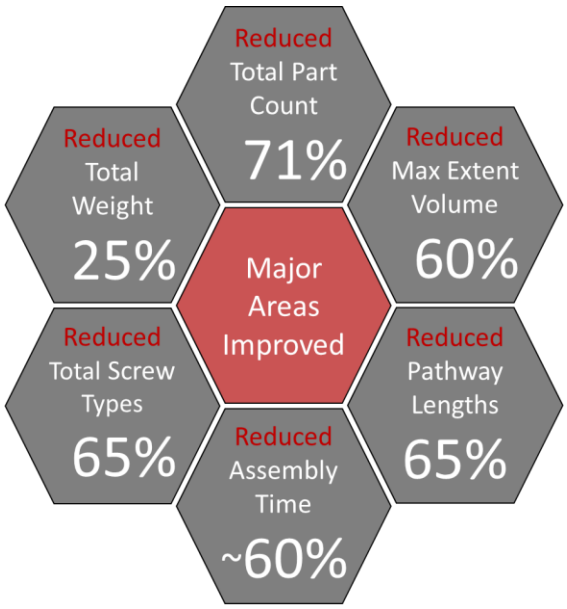

Figure 46: Infographic displaying major areas of improvement of the optimized design.

5.4.1 Volume Reduction

Honeywell initially provided a fuel cell design with a displacement volume of 6,906.31 cm^3. Through the methods used, we successfully reduced this maximum extent volume to 2,832.5 cm^3, achieving a 60% volume reduction. Thes calculations are based on the maximum extent volume of the systems, which does not include the electrical PCB board, the heat exchanger, or the hydrogen tank hardware of either system. This significant volume reduction offers the advantage of ensuring compatibility with a compact fuselage design.

5.4.2 Weight Reduction

To calculate the total weight reduction between the two designs, we weighed each system. The measured dry weight of the original system was 1,191.72 grams and the measured dry weight of the optimized system was 896.6 grams. The optimized system successfully reduced the total dry weight by 24.8%. These calculations are based on the total measured weight of the systems, not including the electrical PCB board, the heat exchanger, or the hydrogen tank hardware of either system.

5.4.3 Pathway Reduction

To calculate the total pathway reduction, we analyzed the lengths of each pathway for the original and optimized system designs. Using our nodal analysis, we measured the lengths of

pathways in CAD space. The bar graph in Figure 47 compares the total lengths of pathways in the original and optimized systems for each loop. One of the goals of reducing the pathway lengths was to reduce pressure loss.

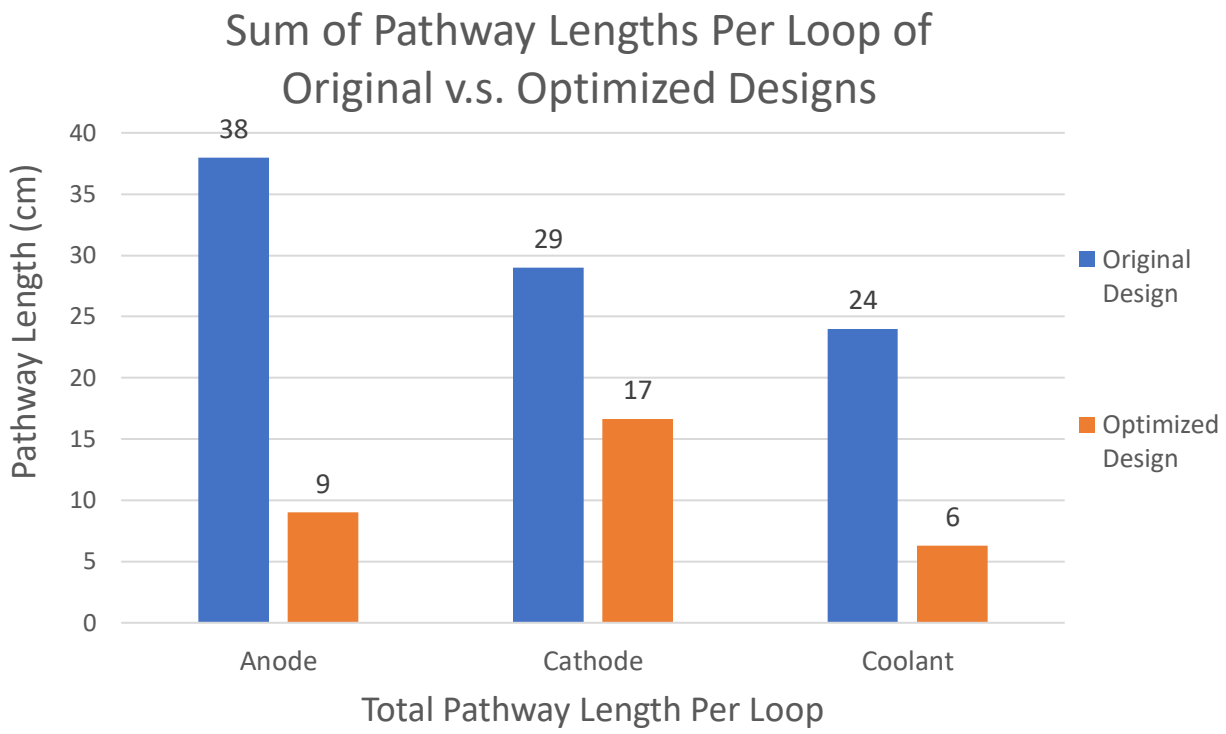

Figure 47: Comparison of pathway length totals between designs for each loop.

The total lengths of the pathways in each loop were combined to calculate the total reduction in pathway length. The original design contained a total pathway length of 91 centimeters and the optimized design contained a total pathway length of 32 centimeters, resulting in a total reduction of 64.9%. These calculations do not include the pathways to and from the heat exchanger (L2C-L3A, L3B-L4A) or the pathway from the tank hardware to the system (A1B-A2A), as these pathways were not considered part of the system for comparison.

5.4.4 Part Count, Screw Types, and Assembly Hours

Based on the assembly guide that Honeywell provided to us for the 600W system, the original part count was about 221 parts. Our new assembly with the manifolds has 65 total parts, meaning we reduced this part count by 70.5%.

Additionally, the new design allows for much easier assembly with more standardized hardware, which requires less variety of tools. The original design utilized 17 different types of screws, while the optimized design only requires 17, resulting in a 64.7% reduction in screw types.

The reduction in part count and hardware standardization reduces labor costs for assembly, allowing customers to assemble the fuel cell system much more efficiently when they receive it. Based on rough estimations of time associated with the complete assembly of the original and optimized system designs, the reduction of assembly time was reduced by about 60%. This considered an estimated 150 minutes to assemble the original design and an estimated 60 minutes to assemble the optimized design.

Based on the data above, the team successfully reduced maximum extent volume, weight, part count, screw types, and assembly time for the fuel cell system. Through thorough testing of the system, we validated that our design has the potential to run at the full 600-watt power with some adjustments for leakage.

6. Discussion

6.1 Limitations

Although our project was successful overall, there were several aspects that posed limitations to the success of our project at its conclusion. These posed challenges that Honeywell should consider if this project is continued in the future.

6.1.1 Challenges with Maintenance

As the manifold is printed in two parts on either side of the fuel cell stack, there is little room for maintenance changes to be made within each part. Since there are so many components included in one single part for each of the manifolds, if a section of a part is broken or damaged, it would likely require the entire part to be re-printed. This would make maintenance take longer, since the 3D printing company would have to be contacted for the part to be reprinted. Reprinting and procuring the part using nylon multi-jet fusion may take between 2-5 business days to complete. This adds another layer of contact required for getting the part.

6.1.2 Adaptability to Other Applications

Although the manifold design reduces the number of parts and maximum extent volume of the entire fuel cell system, it might be difficult to adapt these exact pieces to other applications because they are so uniquely designed for this system. Some design tools and methods may be applied to Honeywell's 1200W system and other applications where multiple components must be made condensed or combined.

6.1.3 Difficulty of Assembly

The manifold was designed to optimize volume and weight, resulting in a minimum amount of negative space where tools can reach. In the blower ballast manifold, there were multiple hard to reach screws that attached the fan to the fan housing. This lack of clearance is due to adequate ballast space. When assembling the fuel cell using the manifold, screws are required to fasten parts, and some may be difficult to reach during assembly because of the limited amount of space for tools. Another obstacle with assembly is due to the minor shrinkage of nylon printed parts. This results in some internal pathways and entrances to the manifold being slightly too narrow for the connecting parts.

6.1.4 Accessibility to Residual Nylon Powder

The intricate design layouts of the manifolds are accompanied by the challenge of accessing internal pathways and clearing excess nylon powder. In the assembly process, tools such as metal brushes and compressed air were used to clear loose nylon powder within the manifold. This can be difficult to achieve due to pathways being located without adequate clearance. Small tools are required to access these hard-to-reach pathways and clear the powder. In our design we added access pathways that allow the loose nylon powder to be dislodged, but the internal geometry of the part still made it difficult to extract all of it. Ball bearings are also helpful for this challenge when placed inside paths and holes following the clearing process. These were used on the blower and ballast manifold to better clean out excess powder. With this challenge in mind, multiple design iterations were created to provide as much clearance as possible without compromising the optimization.

6.2 Design and Manufacturing Recommendations

Considering the limitations we have listed above; the team proposed some manufacturing and design recommendations based on the design process and the knowledge we have acquired. The team suggests that Honeywell continues to use nylon MultiJet printing for creating these manifold pieces because of the tight tolerances and advantages of the material, which allowed for ideal fits. Although this method is unique and an outside printing company is required, this 3D printing technique is highly advantageous to the design.

Although nylon MultiJet printing has proven to be very advantageous for our project, allowing for tight tolerances, smooth finishes, and water and heat resistant surfaces, there are some limitations. The biggest limitation is the difficulty in getting the loose nylon powder out of material, especially in tight, hard to reach pathways. One method to remedy this is to add more access holes and to keep this factor in mind when designing any type of manifold. This type of 3D printing is ideal for this application, but it is crucial to understand the process and be prepared to adjust accordingly.

Another manufacturing recommendation is to further standardize hardware where it is possible. One major limitation for the original Honeywell assembly was the plethora of different hardware, thus requiring a large variety of tools, making the assembly process more complicated.

In our design, we have reduced the variety of hardware, but there is still room for improvement to further streamline hardware and assembly.

The PCB mounting frame and support stand can be manufactured using traditional FDM or resin 3D printing. Our team used resin for these prints, which we recommend based on the strength and smooth finishes. Although FDM printing is slightly cheaper, Honeywell may find resin printing more appealing in the long term. However, since tolerancing does not need to be as tight for these specific parts compared to the manifold pieces, FDM printing would be sufficient.

Finally, we suggest that Honeywell create an assembly guide based on the Bill of Materials and order of assembly we have developed for our design. This order of assembly is based on the easiest and most logical way to assemble components. Therefore, Honeywell's customers will benefit from an assembly guide offering the most efficient assembly methods.

7. Conclusion

Throughout this project, our team developed techniques and practices to improve and refine our design process. We leveraged additive manufacturing techniques to tailor our design to meet our goals. We improved the design of Honeywell's 600W hydrogen fuel cell system to better fit the needs of their customers by enhancing the experience of assembly and significantly reducing weight and volume metrics.

7.1 Project Impact

The impact of this project extends far beyond the optimization of Honeywell Aerospace's hydrogen PEM fuel cell design. There are broader economic, environmental, and societal impacts as a byproduct of the further advancement of fuel cell technology. In the following section, we will discuss a few ways in which the improvement of PEMFC technologies offer evolutionary benefits to the planet.

7.1.1 Economic Impact

There is a significant economic impact of using 3D printed manifolds over traditional, multi-part assemblies. This is primarily due to the nature of 3D prints being composed of a single material with minimal fasteners and connections. The use of additive manufacturing allows designers to utilize complex geometry in their designs without exhibiting high manufacturing and production costs. The optimized manifold design also offers benefits from a manufacturability standpoint. For example, the ability to create custom parts is limitless, as manifolds can be specifically tailored to meet unique design needs. Additionally, by consolidating multiple components into a single 3D printed part, the need for additional hardware such as fasteners, gaskets, mounting plates, and tubing is tremendously reduced. The labor hours necessary to assemble the fuel cell system are also greatly reduced, as is the potential for human errors during assembly. This contributes to a major reduction in costs including reduced labor costs, reduced material costs for hardware, and reduced tooling costs because of more standardized hardware types (Attaran, 2017).

Beyond the economic benefit to Honeywell, using a 3D printed manifold offers economic benefits on a much larger scale. The use of 3D printing can impact a wide array of economic facets from production and logistics to high-tech job growth (*Honeywell Aerospace and NREL*

Partner To Scale Novel Hydrogen Fuel Storage Solution for Drones, n.d.). Given the decrease in the number of parts to manufacture and labor to provide for assembly, production facilities invest more money into innovative designs and technologies. Furthermore, more standardized components mean less tooling, spare parts, and necessary storage to support mass production. Although it appears that additive manufacturing would replace the need for workers, it would rather require manufacturers to advance their skills in the utilization and maintenance of 3D printers.

7.1.2 Environmental Impact

The further development of hydrogen-based proton exchange membrane fuel cell systems offers greater environmental impacts, especially on clean energy and sustainability. Optimizing Honeywell's 600W PEMFC increases the energy production of the fuel cell, thus providing increased power efficiency and offering a feasible sustainable energy option (Edwards et al., 2008). In this specific case, the PEMFC will be used in unmanned aerial vehicles (UAVs), allowing them to maintain longer flight times with the same source of hydrogen. Parasitic power will also be reduced as the hydrogen source is optimized. This reduction in the system's weight and volume is also beneficial to waste reduction. The utilization of additive manufacturing methods also results in less wasted materials, given that there will be less manufacturing needs for extra components, and therefore, a minimized environmental impact because of manufacturing waste.

From a broader perspective, the improvement of PEMFC systems supports the diversification of energy sources which can reduce the amount of greenhouse gas emissions created by other energy sources like fossil fuels (Edwards et al., 2008). Although the production and transportation of hydrogen still requires further advancements to improve the environmental crisis, the use of PEMFCs can significantly reduce society's carbon footprint. With the only byproducts being heat and water, these fuel cells offer cleaner energy production methods, eliminating the release of many harmful pollutants created by the combustion of fossil fuels. The use of hydrogen for creating electricity offers a more sustainable energy source that is not dependent on harmful processes like fracking and mining.

7.1.3 Societal Impact

In addition to the tremendous economic and environmental impacts, the advancements in PEMFCs also provide many societal benefits, such as improved transportation systems and emergency services. For example, the use of PEMFCs in UAVs only touches the surface of their potential utilization in electric vehicles. As discussed before, they are becoming increasingly popular in hybrid and electric cars and could soon be integrated into much larger vehicles in the future, such as aircraft or even spacecraft. Using fuel cell systems can provide much faster, cheaper, and more sustainable transportation options (*Honeywell Aerospace and NREL Partner To Scale Novel Hydrogen Fuel Storage Solution for Drones*, n.d.).

Another major societal implementation of these PEMFCs is in emergency situations when supplies must be shipped in a timely manner during a crisis. For example, when natural disasters occur due to powerful storms, volcanic eruptions, or earthquakes, it is very difficult for emergency services to reach impacted communities with necessary supplies and services. Using PEMFCs to ship essential aid to these communities offers a major improvement to emergency response times and could help save many lives (*Using Drones to Deliver Critical Humanitarian Aid*, n.d.).

Furthermore, their use in unmanned aerial vehicles, such as drones, would enhance our experience with delivery services. These vehicles can ship packages to people's doors much more efficiently than a truck would. Along with this, using fuel cell powdered drones instead of delivery trucks would greatly reduce carbon dioxide emissions from constant driving (Honeywell Hydrogen Fuel Cell, n.d.).

Ultimately, we find ourselves at the early stages of unlocking the variety of potentials of fuel cells. From enhancing sustainability through clean energy to benefiting society during crises, opportunities for advancements and benefits cross various industries.

7.2 Future Work

Although our team could run power through the fuel cell system and see how well it would function, we could not hook the fuel cell up to an actual UAV. Future work should focus on further testing the prototypes in Honeywell's small aerial drones to assess how well the design fits in the drone, how efficiently the drone can fly, and where the design can be improved.

Along with further testing, the design can be adjusted for Honeywell's 1200W system as well. Our design of this serves to specifically function within Honeywell's 600W UAV system.

However, there is also an opportunity to utilize these same techniques to optimize the company's much larger 1200W UAV system. By employing similar design methods in which weight and volume reduction are prioritized and hardware is standardized, along with the use of additive manufacturing tools, Honeywell can create a similar, compact manifold design for this larger system. This can potentially reduce weight and volume and make the 1200W system more efficient.

Additionally, future work could also be investigating the potential use of nTop, a software that can be used to optimize designs based on modeling tools and design criteria. nTop can optimize designs based on heat, pressure, and other simulation data to create a design that exceeds performance targets. It also provides real-time feedback, and it can generate hundreds of variations within minutes using GPU acceleration. The software also offers a "lightweighting" application, in which it attempts to achieve the highest possible weight reduction while maintaining strength and structural integrity. nTop's lightweighting feature and optimization tools can be employed in our design to improve the fuel cell's efficiency even further. Software such as nTop should be explored by future teams to take our design even further (Next-Gen Engineering Design Software, n.d.).

Engineering standards and regulations are at the forefront of safety and welfare when creating something new or innovating upon an existing design. Honeywell will have to consider some engineering standards when pursuing and implementing this new fuel cell system design. One might be ISO/AWI 25009, which outlines the general requirements and test methods for hydrogen fuel gas pipes of gaseous hydrogen fuel cell powered UAVs (*ISO/AWI 25009*, n.d.). Along with this, ISO/TC 197 should be investigated, which outlines the standardization in the field of systems and devices for the production, storage, transport, measurement, and use of hydrogen (*ISO/TC 197 - Hydrogen Technologies*, 2022). ASTM D7606-17 outlines the standard practices for the sampling of fuel cell feed gases (*Standard Practice for Sampling of High Pressure Hydrogen and Related Fuel Cell Feed Gases*, n.d.), which would also be necessary to comply with. Among these engineering standards, future work should consider whether these fuel cell systems will be sold in the United States, or internationally, which will impact which standards need to be upheld. This will properly ensure the safety and standard adherence of the product.

Based on the future work outlined above, our team is confident that the versatile design and system configuration can eventually be integrated into Honeywell's fuel cell systems for UAVs and other applications. With sustained effort, our project holds the potential to benefit across multiple industries while significantly contributing to environmental and social welfare.

References

ASME Constitution. (2012). *Code of Ethics of Engineers* (Article C2.1.1). https://www.asme.org/

Attaran, M. (2017). The rise of 3-D printing: The advantages of additive manufacturing over traditional manufacturing. Business Horizons, 60(5), 677–688. https://doi.org/10.1016/j.bushor.2017.05.011

Bayer Material Science LLC (n.d.). Annular Snap Joint Example [Photograph]. MIT Fab Lab, https://fab.cba.mit.edu/classes/S62.12/people/vernelle.noel/Plastic_Snap_fit_design.pdf

Bayer Material Science LLC (n.d.). Cantilever Snap Joint Example [Photograph]. MIT Fab Lab, https://fab.cba.mit.edu/classes/S62.12/people/vernelle.noel/Plastic_Snap_fit_design.pdf

Edwards, P. P., Kuznetsov, V. L., David, W. I. F., & Brandon, N. P. (2008). Hydrogen and fuel cells: Towards a sustainable energy future. Foresight Sustainable Energy Management and the Built Environment Project, 36(12), 4356–4362. https://doi.org/10.1016/j.enpol.2008.09.036

Guerrero Moreno, N., Cisneros Molina, M., Gervasio, D., & Pérez Robles, J. F. (2015). Approaches to polymer electrolyte membrane fuel cells (PEMFCs) and their cost. Renewable and Sustainable Energy Reviews, 52, 897–906. https://doi.org/10.1016/j.rser.2015.07.157

Honeywell Aerospace and NREL Partner To Scale Novel Hydrogen Fuel Storage Solution for Drones. (n.d.). Retrieved April 11, 2024, from https://www.nrel.gov/news/program/2023/honeywell-aerospace-and-nrel-partner-to-scale-novel-hydrogen-fuel-storage-solution-for-drones.html

Honeywell Hydrogen Fuel Cell. (n.d.). Retrieved April 10, 2024, from https://aerospace.honeywell.com/us/en/products-and-services/product/hardware-and-systems/honeywell-hydrogen-fuel-cell

Honeywell International Inc. (2021). *600U Hydrogen Fuel Cell*. Honeywell Aerospace. https://aerospace.honeywell.com/content/dam/aerobt/en/documents/learn/products/electric-power/infographics/N61-3014-000-000_HydrogenFuelCell_600U_v5_pr.pdf

ISO/AWI 25009. (n.d.). ISO. Retrieved April 11, 2024, from https://www.iso.org/standard/88779.html

ISO/TC 197—Hydrogen technologies. (2022, September 28). ISO. https://www.iso.org/committee/54560.html

Kraytsberg, A., & Ein-Eli, Y. (2014). Review of Advanced Materials for Proton Exchange Membrane Fuel Cells. *Energy & Fuels*, *28*(12), 7303-7330.

MIT Fab Lab & Bayer MaterialScience LLC. (n.d.). Snap-Fit Joints for Plastics. https://fab.cba.mit.edu/classes/S62.12/people/vernelle.noel/Plastic_Snap_fit_design.pdf

Next-Gen Engineering Design Software: nTop (formerly nTopology). (n.d.). nTop. Retrieved April 10, 2024, from https://www.ntop.com/

O'Connor, H. J., Dickson, A. N., & Dowling, D. P. (2018). Evaluation of the mechanical performance of polymer parts fabricated using a production scale multi jet fusion printing process. Additive Manufacturing, 22, 381–387. https://doi.org/10.1016/j.addma.2018.05.035

Optimization of manifold design for 1 kW-class flat-tubular solid oxide fuel cell stack operating on reformed natural gas. (2016). Journal of Power Sources, 327, 638–652. https://doi.org/10.1016/j.jpowsour.2016.07.077

Standard Practice for Sampling of High Pressure Hydrogen and Related Fuel Cell Feed Gases. (n.d.). Retrieved April 11, 2024, from https://www.astm.org/d7606-17.html

Stanford.edu. (n.d.). *Proton Exchange Membrane Schematic*. PEM Fuel Cells. Retrieved October 9, 2023, from https://web.stanford.edu/group/frankgroup/research_topic_3.html.

Using drones to deliver critical humanitarian aid. (n.d.). WFP Drones. Retrieved April 11, 2024, from https://drones.wfp.org/updates/using-drones-deliver-critical-humanitarian-aid

Wang, T., Qiu, Y., Xie, S., Li, Q., Chen, W., Breaz, E., Ravey, A., & Gao, F. (2024). Energy Management Strategy Based on Optimal System Operation Loss for a Fuel Cell Hybrid Electric Vehicle. *IEEE Transactions on Industrial Electronics*, *71*(3), 2650–2661. https://doi.org/10.1109/TIE.2023.3269477

Appendices

A: Nodal Language

I. Nodal Code Key

Nodal Code Key							
Code	Node	Letter 1	Loop	Number	Subcomponent	Letter 2	Inlet/Outlet
C1A	Humidifier Inlet A	C	CATHODE	1	HUMIDIFIER	A	INLET
C1B	Humidifier Outlet B	C	CATHODE	1	HUMIDIFIER	B	OUTLET
C1C	Humidifier Inlet C	C	CATHODE	1	HUMIDIFIER	C	INLET
C1D	Humidifier Outlet D	C	CATHODE	1	HUMIDIFIER	D	OUTLET
C2A	Blower Inlet	C	CATHODE	2	BLOWER	A	INLET
C2B	Blower Outlet	C	CATHODE	2	BLOWER	B	OUTLET
C3A	Air Filter Inlet	C	CATHODE	3	AIR FILTER	A	INLET
C3B	Air Filter Outlet	C	CATHODE	3	AIR FILTER	B	OUTLET
C4	Exhaust	C	CATHODE	4	EXHAUST		
S1A	Stack Inlet A	S	STACK	1	STACK	A	INLET
S1B	Stack Outlet B	S	STACK	1	STACK	B	OUTLET
L1A	Pump Inlet A	L	COOLANT	1	PUMP	A	INLET
L1B	Pump Outlet B	L	COOLANT	1	PUMP	B	OUTLET
L2A	Bypass Valve Inlet A	L	COOLANT	2	BYPASS VALVE	A	INLET
L2B	Bypass Valve Outlet B	L	COOLANT	2	BYPASS VALVE	B	OUTLET
L2C	Bypass Valve Outlet C	L	COOLANT	2	BYPASS VALVE	C	OUTLET
L3A	Heat Exchanger Inlet	L	COOLANT	3	HEAT EXCHANGER	A	INLET
L3B	Heat Exchanger Outlet	L	COOLANT	3	HEAT EXCHANGER	B	OUTLET
L4A	Reservoir Inlet	L	COOLANT	4	RESERVOIR	A	INLET
L4B	Reservoir Outlet	L	COOLANT	4	RESERVOIR	B	OUTLET
S1E	Stack Inlet E	S	STACK	1	STACK	E	INLET
S1F	Stack Outlet F	S	STACK	1	STACK	F	OUTLET
A1A	Tank Hardware Inlet	A	ANODE	1	TANK HARDWARE	A	INLET
A1B	Tank Hardware Outlet	A	ANODE	1	TANK HARDWARE	B	OUTLET
A2A	3-Way Solenoid Valve Inlet A	A	ANODE	2	3-WAY SOLENOID VALVE	A	INLET
A2B	3-Way Solenoid Valve Outlet B	A	ANODE	2	3-WAY SOLENOID VALVE	B	OUTLET
A2C	3-Way Solenoid Valve Outlet C	A	ANODE	2	3-WAY SOLENOID VALVE	C	INLET
A3A	Solenoid Valve Inlet A	A	ANODE	3	SOLENOID VALVE	A	INLET
A3B	Solenoid Valve Outlet B	A	ANODE	3	SOLENOID VALVE	B	OUTLET
A4A	Hydrogen Ballast Inlet A	A	ANODE	4	HYDROGEN BALLAST	A	INLET
A4B	Hydrogen Ballast Outlet B	A	ANODE	4	HYDROGEN BALLAST	B	OUTLET
A4C	Hydrogen Ballast Outlet C	A	ANODE	4	HYDROGEN BALLAST	C	OUTLET
A5A	Solenoid Valve Inlet A	A	ANODE	5	SOLENOID VALVE	A	INLET
A5B	Solenoid Valve Outlet B	A	ANODE	5	SOLENOID VALVE	B	OUTLET
A6A	Exhaust	A	ANODE	6	EXHAUST		
S1C	Stack Inlet C	S	STACK	1	STACK	C	INLET
S1D	Stack Outlet D	S	STACK	1	STACK	D	OUTLET
E1A	PCB Inlet	E	ELECTRICAL	1	PCB	A	INLET
E1B	PCB Inlet B	E	ELECTRICAL	1	PCB	B	OUTLET
S1G	Stack Inlet G	S	STACK	1	STACK	G	INLET
S1H	Stack Inlet H	S	STACK	1	STACK	H	OUTLET

II. Nodal Pathways Key

	WPI MQP Naming Conventions									Honeywell Naming Conventions		
Nodal Code	Pathway Name	Start Node	Start Name	End Node	End Name	Loop	Type	Fluid	Part #	Part Name	Part Description
C3A-C3B	Air Filter Inlet to Air Filter Outlet	C3A	Air Filter Inlet	C3B	Air Filter Outlet	Cathode	Component	Air	015-707	MANIFOLD, BLOWER+H2 BALLAST	Blower and Ballast Manifold
C3B-C2A	Air Filter Outlet to Blower Inlet	C3B	Air Filter Outlet	C2A	Blower Inlet	Cathode	Pathway	Air	015-707	MANIFOLD, BLOWER+H2 BALLAST	Blower and Ballast Manifold
C2A-C2B	Blower Inlet to Blower Outlet	C2A	Blower Inlet	C2B	Blower Outlet	Cathode	Component	Air	015-707	MANIFOLD, BLOWER+H2 BALLAST	Blower and Ballast Manifold
C2B-C1A	Blower Outlet to Humidifier Inlet A	C2B	Blower Outlet	C1A	Humidifier Inlet A	Cathode	Pathway	Air	015-707	MANIFOLD, BLOWER+H2 BALLAST	Blower and Ballast Manifold
C1A-C1B	Humidifier Inlet A to Humidifier Outlet B	C1A	Humidifier Inlet A	C1B	Humidifier Outlet B	Cathode	Component	Air		HUMIDIFIER	BLOWER TO
C1B-S1A	Humidifier Outlet B to Stack Inlet A	C1B	Humidifier Outlet B	S1A	Stack Inlet A	Cathode	Pathway	Air	015-708	MANIFOLD, COOLANT	Pump and Cathode Manifold
S1A-S1B	Stack Inlet A to Stack Outlet B	S1A	Stack Inlet A	S1B	Stack Outlet B	Cathode	Component	Air		STACK	HUMIDIFIER TO HUMIDIFIER
S1B-C1C	Stack Outlet B to Humidifier Inlet C	S1B	Stack Outlet B	C1C	Humidifier Inlet C	Cathode	Pathway	Air	015-708	MANIFOLD, COOLANT	Pump and Cathode Manifold
C1C-C1D	Humidifier Inlet C to Humidifier Outlet D	C1C	Humidifier Inlet C	C1D	Humidifier Outlet D	Cathode	Component	Air		HUMIDIFIER	STACK TO EXHAUST
C1D-C4	Humidifier Outlet D to Exhaust	C1D	Humidifier Outlet D	C4	Exhaust	Cathode	Pathway	Air	015-707	MANIFOLD, BLOWER+H2 BALLAST	Blower and Ballast Manifold
L1A-L1B	Pump Inlet A to Pump Outlet B	L1A	Pump Inlet A	L1B	Pump Outlet B	Coolant	Component	Coolant		PUMP	Pump and Cathode Manifold
L1B-S1E	Pump Outlet B to Stack Inlet E	L1B	Pump Outlet B	S1E	Stack Inlet E	Coolant	Pathway	Coolant	015-708	MANIFOLD, COOLANT	Pump and Cathode Manifold
S1E-S1F	Stack Inlet E to Stack Outlet F	S1E	Stack Inlet E	S1F	Stack Outlet F	Coolant	Component	Coolant		STACK	S1
S1F-L2A	Stack Outlet F to Bypass Valve Inlet A	S1F	Stack Outlet F to	L2A	Valve Inlet A	Coolant	Pathway	Coolant	015-708	MANIFOLD, COOLANT	Pump and Cathode Manifold
L2A-L2B	Bypass Valve Inlet A to Bypass Valve Outlet B	L2A	Bypass Valve Inlet A	L2B	Valve Outlet B	Coolant	Component	Coolant		BYPASS VALVE	L2
L2A-L2C	Bypass Valve Inlet A to Bypass Valve Outlet C	L2A	Bypass Valve Inlet A	L2C	Valve Outlet C	Coolant	Component	Coolant		BYPASS VALVE	L2
L2B-L4A	Bypass Valve Outlet B to Reservoir Inlet A	L2B	Bypass Valve Outlet B	L4A	Reservoir Inlet A	Coolant	Pathway	Coolant	015-708	MANIFOLD, COOLANT	Pump and Cathode Manifold
L2C-L3A	Bypass Valve Outlet C to Heat Exchanger Inlet A	L2C	Bypass Valve Outlet C	L3A	Exchanger Inlet A	Coolant	Pathway	Coolant		RUBBER TUBING	EXTERNAL
L3A-L3B	Heat Exchanger Inlet A to Heat Exchanger Outlet B	L3A	Heat Exchanger Inlet A	L3B	Heat Exchanger Outlet B	Coolant	Component	Coolant		HEAT EXCHANGER	EXTERNAL
L3B-L4A	Heat Exchanger Outlet B to Reservoir Inlet A	L3B	Heat Exchanger Outlet B	L4A	Reservoir Inlet A	Coolant	Pathway	Coolant		RUBBER TUBING	EXTERNAL
L4A-L4B	Reservoir Inlet A to Reservoir Outlet B	L4A	Reservoir Inlet A	L4B	Reservoir Outlet B	Coolant	Component	Coolant	015-708	MANIFOLD, COOLANT	Pump and Cathode Manifold
L4B-L1A	Reservoir Outlet B to Pump Inlet A	L4B	Reservoir Outlet B	L1A	Pump Inlet A	Coolant	Pathway	Coolant	015-708	MANIFOLD, COOLANT	Pump and Cathode Manifold
A1A-A1B	Tank Hardware Inlet to Tank Hardware Outlet	A1A	Tank Hardware Inlet	A1B	Tank Hardware Outlet	Anode	Component	H2 Gas		H2 TANK	
A1B-A2A	Tank Hardware Outlet to 3-Way Solenoid Valve Inlet A	A1B	Tank Hardware Outlet	A2A	3-Way Solenoid Valve Inlet A	Anode	Pathway	H2 Gas	015-707	MANIFOLD, BLOWER+H2 BALLAST	INCLUDING RUBBER TUBING
A2A-A2B	3-Way Solenoid Valve Inlet A to 3-Way Solenoid Valve Outlet B	A2A	3-Way Solenoid Valve Inlet A	Z	3-Way Solenoid Valve Outlet B	Anode	Component	H2 Gas		SOLENOID VALVE	3 VALVES, 3-WAY
A2B-S1C	3-Way Solenoid Valve Outlet B to Stack Inlet C	A2B	3-Way Solenoid Valve Outlet B	S1C	Stack Inlet C	Anode	Pathway	H2 Gas	015-707	MANIFOLD, BLOWER+H2 BALLAST	Blower and Ballast Manifold
S1C-S1D	Stack Inlet C to Stack Outlet D	S1C	Stack Inlet C	S1D	Stack Outlet D	Anode	Component	H2 Gas		STACK	S1
S1D-A3A	Stack Outlet D to Solenoid Valve Inlet A	S1D	Stack Outlet D	A3A	Solenoid Valve Inlet A	Anode	Pathway	H2 Gas	015-707	MANIFOLD, BLOWER+H2 BALLAST	Blower and Ballast Manifold
A3A-A3B	Solenoid Valve Inlet to Solenoid Valve Outlet	A3A	Solenoid Valve Inlet	A3B	Solenoid Valve Outlet	Anode	Component	H2 Gas		SOLENOID VALVE	2 VALVES, 2-WAY
A3B-A4A	Solenoid Valve Outlet to Hydrogen Ballast Inlet	A3B	Solenoid Valve Outlet	A4A	Hydrogen Ballast Inlet	Anode	Pathway	H2 Gas	015-707	MANIFOLD, BLOWER+H2 BALLAST	Blower and Ballast Manifold
A4A-A4B	Hydrogen Ballast Inlet to Hydrogen Ballast Outlet B	A4A	Hydrogen Ballast Inlet	A4B	Hydrogen Ballast Outlet B	Anode	Component	H2 Gas	015-707	MANIFOLD, BLOWER+H2 BALLAST	Blower and Ballast Manifold
A4B-A5A	Hydrogen Ballast Outlet B to Solenoid Valve Inlet	A4B	Hydrogen Ballast Outlet B	A5A	Solenoid Valve Inlet	Anode	Pathway	H2 Gas	015-707	MANIFOLD, BLOWER+H2 BALLAST	Blower and Ballast Manifold
A5A-A5B	Solenoid Valve Inlet to Solenoid Valve Outlet	A5A	Solenoid Valve Inlet	A5B	Solenoid Valve Outlet	Anode	Component	H2 Gas		SOLENOID VALVE	1 VALVE, 2-WAY
A5B-A6A	Solenoid Valve Outlet to Exhaust	A5B	Solenoid Valve Outlet	A6	Exhaust	Anode	Pathway	H2 Gas	015-707	MANIFOLD, BLOWER+H2 BALLAST	Blower and Ballast Manifold
A4C-A2C	Hydrogen Ballast Outlet C to 3-Way Solenoid Valve Inlet C	A4C	Hydrogen Ballast Outlet C	A2C	3-Way Solenoid Valve Inlet C	Anode	Pathway	H2 Gas	015-707	MANIFOLD, BLOWER+H2 BALLAST	Blower and Ballast Manifold
E1A-E1B	Printed Circuit Board (PCB)	E1A	PCB Inlet	E1B	PCB Outlet	Electrical	Component	Electrons		PRINTED CIRCUIT BOARD	E1
	PCB Mounting Plate				PCB Mounting Plate	Hardware	Component		015-710	MOUNTING PLATE, PCB	PCB Mounting Plate
	System Stand					Hardware	Component		015-709	STAND, 600W PRINTED SYSTEM	Mike's Stand

KEY	DEFINITION
	Honeywell's # - component
	Cathode Components
	Coolant Components
	Anode Components
	Cathode Pathways
	Coolant Pathways
	Anode Pathways

III. Bill of Materials - Optimized System

Bill of Materials Optimized System						
Item #	QTY	PART #	Part Name	Description	Type	Manifold
1	1	015-707	MANIFOLD, BLOWER+H2 BALLAST	Blower and Ballast Manifold	3D Printed	(BB)
2	1	015-708	MANIFOLD, COOLANT	Pump and Cathode Manifold	3D Printed	(PC)
3	1	R70700600-1	600W STACK ASSEMBLY	Fuel Cell Stack	Honeywell Part	N/A
4	1	R70700635-1	ASSEMBLY, HUMIDIFIER, 600W	Humidifier	Honeywell Part	N/A
5	1	R70700611-1	BLOWER ASSY	Blower Assembly	Honeywell Part	BB
6	1	R70700645-1	ASSEMBLY, ANODE PURGE	Solenoid Valve Assembly	Honeywell Part	BB
7	1	R70700626-1	BYPASS VALVE	Diverter Valve	Honeywell Part	PC
8	1	R70700626-1	COOLANT PUMP	Coolant Pump	Honeywell Part	PC
9	6	96817A906	M3 X 6, Self Tapping Screws	M3, 6mm length (for blower mount)	McMaster	BB
10	4	96817A910	M3 X 10 Self Tapping Screws	M3, 10mm length (2 bypass, 2 pump)	McMaster	PC
11	12	91772A059	rounded head screws, 0-80 thread	Solenoid Valve Screws	McMaster	BB
12	2	9587K11	1/8" OD Ball Bearings	1/8"OD (for sealing blow-out holes)	McMaster	BB
13	4	92196A089	18-8 Stainless Steel Socket Head Screw	2-56 Thread Size, 1-1/8" Long (for mounting P/C Manifold to FCS)	McMaster	PC
14	4	HONEYWELL	2-56 Thread Size, 9/16"	2-56 x 9/16" (for mounting B/B to FCS)	Honeywell Part	BB
15	1	2958N16	1/2" ID Sealing Plug	1/2" ID (seals hole on top of ballast)	McMaster	BB
16	1	AMAZON	AIR FILTER	(1.35in x 1.06 in carbon fiber)	Amazon	BB
17	1	HONEYWELL	O-RING		Honeywell Part	PC
18	4	HONEYWELL	SOLENOID VALVE MOUNTING BRACKET		Honeywell Part	BB
19	2	HONEYWELL	RUBBER GASKETS	Seals both manifolds to FCS	Honeywell Part	BB/PC
20	3	HONEYWELL	PRESSURE SENSOR SCREWS		Honeywell Part	BB
21	3	HONEYWELL	RUBBER TUBING	from H2 Tank	Honeywell Part	BB/PC
22	1	HONEYWELL	HYDROGEN TANK	H2 Tank Hardware	Honeywell Part	N/A
23	1	015-709	STAND, 600W PRINTED SYSTEM	Mike's Stand	3D Printed	N/A
24	1	015-710	MOUNTING PLATE, PCB	PCB Mounting Plate	3D Printed	N/A
25	1	014-411	ELECTRONICS BOARD ASSY	Electronic PCB	Honeywell Part	N/A
26	1	R70700669-1	ASSEMBLY, HEAT EXCHANGER	Heat Exchanger	Honeywell Part	N/A